

Chapter 2

Slag Infiltration, Lubrication and Frictional Forces

Abstract It is essential to lubricate the shell since inadequate lubrication leads to defects in the steel product (e.g. longitudinal cracks, sticker breakouts and star cracks). The liquid layer of the slag film, formed between the shell and the mould, lubricates the newly formed shell; the lubrication increases with increasing liquid slag thickness (d_l). Lubrication is usually represented by the powder consumption (Q_s in units of kg slag (or powder) m^{-2}) which is related to liquid film thickness (d_l). However, there are several terms used for powder consumption and these terms are interrelated (e.g. Q_s , Q_t and Q_{MR}). The frictional forces acting on the shell are highest in the centre of slabs and thus slabs need more lubrication. The required powder consumption, Q_s increases with increasing distance from the corner and thus $Q_s^{\text{slab}} > Q_s^{\text{bloom}} > Q_s^{\text{billet}}$. The *required* powder consumption can be calculated from the relation, $Q_s^{\text{req}} = 2/(R^* - 5)$ where $R^* = \{2(w + t)/w \cdot t\} =$ (surface area/volume) of the mould. However, the powder consumption, Q_s , is also affected by other parameters, namely, the casting speed (V_c), slag viscosity (η), the break temperature of the slag and the oscillation frequency (f) and stroke (s). There is general agreement that Q_s decreases with increasing casting speed and viscosity (e.g. empirical rules, $Q_s^{\text{slag}} = 0.55/\eta^{0.5} \cdot V_c$). There is some dispute with regard to the effect of f , s and T_{br} but most plant studies indicate that Q_s^{slag} decreases as f , s and T_{br} increase. The *required* values of powder consumption and viscosity can be calculated for the given casting conditions using empirical rules. The predictions of a mathematical model indicate that slag infiltration into the model/ strand channel occurs when the mould and slag rim are descending but little powder consumption occurs when the mould is ascending. The changes in mould direction are accompanied by periods of *confused flow* in the mouth of the channel and little slag infiltration occurs in these periods. Frictional forces and the factors affecting them are also discussed; it was found that liquid friction increased with increasing mould dimensions, slag viscosity, casting speed and ($V_m - V_c$). Plots of liquid friction (F_l) versus casting speed exhibit a minimum since F_l increases with increasing V_c but decreases with decreasing ($V_m - V_c$).

Symbols, Abbreviations and Units

A	Area (m^2)
$\%C_{\text{free}}$	Percentage of free carbon
$\%C_{\text{total}}$	Percentage of total carbon
$\%LOI$	Percentage of loss on ignition
D_C	Mean particle size of the carbon
D_{com}	Distance mould corner to centre (m)
D_l	Thickness of liquid slag film (m)
F_l	Frictional force (N)
f	Frequency (Hz or cycles min^{-1})
f^*	Fraction of powder forming slag
Q_{cycle}	Powder consumption ($\text{kg m}^{-1} \text{ cycle}^{-1}$)
Q_{MR}	Melting rate (kg/min or kg/s)
Q_s	Powder consumption (kg/m^2)
Q_t	Powder consumption (kg/tonne^{-1})
R^*	Mould (surface area/volume) (m^{-1})
s	Stroke length (m)
T	Temperature ($^{\circ}\text{C}$)
T_{br}	Break (or solidification) temperature
t	Time (s) or thickness of mould (m)
t_{cycle}	Time for one cycle (s or min)
t_n	Negative strip time (s)
t_p	Positive strip time (s)
V_c	Casting speed (m/min)
V_m	Velocity of mould (m/min or m/s)
w	Width of mould
η	Slag viscosity (dPas)
ρ	Density (kg/m^3)

Superscripts

^{powd}	Refers to powder
^{slag}	Slag formed from powder

2.1 Introduction

The newly formed steel shell is lubricated as it progresses down the mould by a flow of liquid slag from the slag pool (Fig. 2.1). This flow of slag helps to reduce the frictional forces acting on the shell. The liquid frictional force (F_l) operating on the shell can be calculated using Eq. 2.1 where V_m and V_c are the velocities of the mould and the casting speed, respectively, A is the active surface area of the mould, η = slag viscosity and d_l is the liquid slag film thickness.

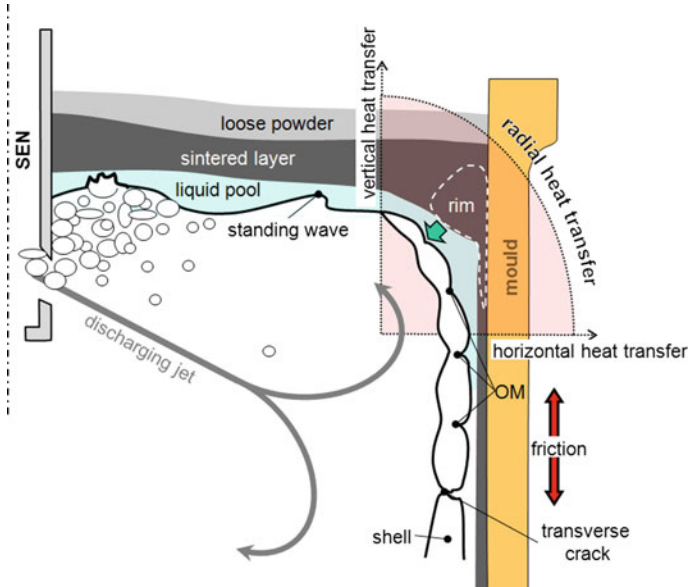


Fig. 2.1 Schematic drawing showing the lubrication of the sausage-shaped shell by liquid slag, which is shown in light blue (permission granted, ISS/AIST, [1])

$$F_l = A\eta(V_m - V_c)/d_l \quad (2.1)$$

Thus the liquid frictional force decreases as the:

- Thickness of the liquid film increases.
- Surface area of the mould decreases.
- Viscosity decreases.
- With a decrease in the difference between the velocities of mould and steel strand.

It will be seen below that the thickness of the liquid slag film (d_l) is related to the powder consumption Q_s (with units of kg/m^2). In addition to the liquid friction forces there are also solid friction forces which tend to occur in the lower mould.

The powder consumption, Q_s (in kg/m^2 of mould) is often used as a measure of the lubrication supplied by the liquid slag since it is linearly related to d_l (see Eq. 2.4).

2.2 Powder Consumption (Q)

The powder consumption (Q) can be expressed in several ways, each term having different units. The most common form for powder consumption is Q_t (in kg/t steel) which is the mass of powder consumed per tonne of steel cast. This provides a measure of the cost of the casting powders in continuous casting.

It should be pointed out that the mould powder contains carbon, carbonate and other volatiles which burn off and, hence, do not contribute to lubrication by the slag. Some billet fluxes contain up to 25% free carbon and consequently, it is necessary to differentiate between mould *powder* and *slag*. This is denoted here by attaching the superscripts, ^{powd} and ^{slag}, respectively, to the various consumption terms. It is possible to calculate one term from the other by calculating the fraction of powder forming slag (f^*) by Eq. 2.2 and using either the free carbon ($\%C_{\text{free}}$) and total carbon contents of the powder ($\%C_{\text{total}}$) or alternatively, the loss on ignition ($\%LOI$) which are usually supplied by the powder manufacturer.

$$f^* = [100 - (\%C_{\text{free}}) - \{(44/12)(\%C_{\text{total}} - \%C_{\text{free}})\}]/100 = (100 - \%LOI)/100 \quad (2.2)$$

The powder consumption of slag can be calculated from the relation:

$$Q_t^{\text{slag}} = f^* Q_t^{\text{powd}}. \quad (2.3)$$

2.2.1 Various Powder Consumption Terms

As mentioned above, the powder consumption can be expressed in various ways, each with different units; the various terms can be calculated from one another, e.g. Q_s and Q_t by Eq. 2.4.

$$Q_s^{\text{slag}} (\text{kg/m}^2) = (f^* 7.6 Q_t^{\text{powd}}) / R^* = \rho d_l \approx 2550 d_l. \quad (2.4)$$

where $R^* = (\text{surface area/volume})$ of mould = $\{2(w + t)/w \cdot t$ (and has units of m^{-1}) $w = \text{width of the mould (m)}$, $t = \text{thickness of the mould (m)}$ and $\rho = \text{the density (kg/m}^3\text{) of the molten slag}$, 7.6 is the density of steel in t/m^3 . Equation 2.4 also shows the link between Q_s and the thickness of the liquid slag film (d_l).

Furthermore, the melting rate of the mould powder, $Q_{\text{MR}}^{\text{powd}}$ (in units of kg/min or kg/s) can be calculated from Q_s^{slag} , by Eq. 2.5 where V_c is the casting speed (m/min).

$$Q_{\text{MR}}^{\text{slag}} (\text{kg/s}) = f^* Q_{\text{MR}}^{\text{powd}} = 2(w + t) Q_s V_c / 60 \quad (2.5)$$

The melting rate should match the powder consumption (Q_s) needed to provide good lubrication of the shell. There are a number of variables which affect the melting rate but it is primarily controlled through the free carbon content ($\%C_{\text{free}}$) and the mean particle size of the carbon ($D_{C_{\text{free}}}$) of the powder (i.e. $Q_{\text{MR}}^{\text{slag}} \uparrow$ as $\%C_{\text{free}} \downarrow$ and $D_{C_{\text{free}}} \uparrow$).

The powder consumption per oscillation cycle, $Q_{\text{cycle}}^{\text{slag}}$ (kg/cycle) can be calculated from Q_s via Eq. 2.6 where $f = \text{oscillation frequency (in Hz)}$

$$Q_{\text{cycle}}^{\text{slag}} (\text{kg cycle}^{-1}) = 2(w + t)Q_s V_c / 60f \quad (2.6)$$

All of the above parameters can be derived by considering a liquid slag film of uniform thickness (d_i) distributed around the mould and by assuming $A_{\text{shell}} = A_{\text{mould}}$.

2.2.2 Measurement of Powder Consumption

The powder consumption, Q_i^{powd} , is frequently determined as the number of bags (N) of known mass of casting powder (m) used in the entire cast, for which the total mass of steel cast (m_{steel}) is known. Thus Q_i^{powd} can be calculated ($Q_i^{\text{powd}} = Nm / m_{\text{steel}}$).

Powder consumption rates for different periods during a cast can be determined by measuring the mass of powder dispensed from the hoppers in a known time period. However, these measurements are affected by the height of the powder in the hopper and thus measured rates are affected by recharging the hopper; for true significance, the measurements should refer to the same height of powder in the hopper. There is some variability in the consumption values. Some of this variability probably arises from small variations in the casting conditions (e.g. changes in casting speed) through the cast.

The most precise method for measurement of mould powder consumption, when, for example, performing plant trials with new mould powders, is to use a bucket with known amount of mould powder and count the number of buckets needed for the casting.

Powder consumption data for 32 casts of the same steel under the same conditions (where any casting speed variations were $< \pm 10\%$) is shown in Fig. 2.2. The mean Q_i value was 0.63 kg/t, the maximum range in values was 0.24 kg/t and the uncertainty was calculated as $\pm 12\%$ [1, 2].

Studies where the powder supply was monitored at nine positions between the centre and the edge of the mould showed that consumption (i) was highest at the edge (presumably because it has to feed the narrow face too) and (ii) went through a minimum located midway between the edge and the centre [3].

The powder consumption at different periods of the cast is shown in Fig. 2.3, it can be seen that the powder consumption appears to be higher at the beginning of the cast and gradually decreases to a steady value.

2.2.3 Methods Used to Understand Slag Infiltration Mechanisms

Several techniques have been used to gain an understanding of the mechanisms responsible for slag infiltration, they are:

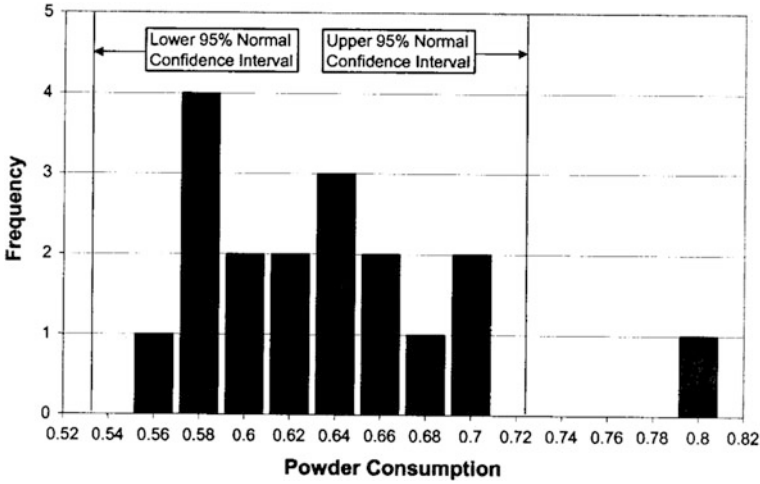


Fig. 2.2 Histogram of powder consumption (kg/t) in similar trials where a variation of $<\pm 10\%$ in casting speed was allowed (*courtesy of Fox [2]*)

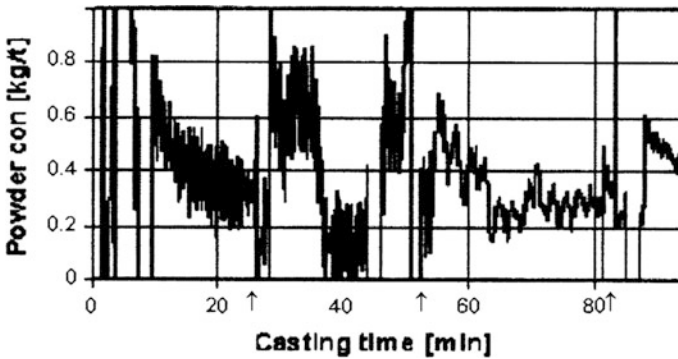


Fig. 2.3 Powder consumption at different periods of the cast (*courtesy Fox [2]*)

2.2.3.1 Analysis of Plant Data

Plant trials are carried out where powder consumption is measured as one variable (for instance, as a function of casting speed or slag viscosity) is changed while all the other variables are held constant. Most of the empirical relations were derived in this manner (see Table 2.3). One major problem with this approach lies in determining the effects of oscillation characteristics where it is common practice to operate with a fixed negative strip ratio. Thus if the frequency is increased, it is common practice to alter the stroke (s) or casting speed to ensure that negative strip time remains the same. Thus there are few plant trial data carried out where only one oscillation parameter (say frequency, f) is varied systematically.

An alternative approach was taken by Saraswat et al. [4]; they carried out a statistical analysis for a large database of powder consumption data from various steel plants in order to identify those variables (V_c , η , f , s , T_{br}) which had a statistically significant effect on Q_s .

2.2.3.2 Physical Modelling Studies

In physical models, the effect of changing one variable is studied by observation of the slag flow. The physical models can be divided into three types, given below, and details of the various studies are given in Table 2.1:

- (a) *Cold (or water) models* which are usually carried out at near-ambient temperatures. In some cases the slag rim is represented by a solid ledge [5] and other cases by freezing of the water representing the slag [6]. The main problem with these tests is that they tend to be isothermal whereas the conditions in the mould are not isothermal.

Table 2.1 Details of some physical modelling studies of slag infiltration and factors affecting powder consumption

Reference	Type	Metal	Slag	Comments, findings
Anzai [12]	CM	Rubber belt	Paraffin	Pressure measured in mould/shell gap; mould = oscillating plate, shell = moving belt
Jenkins [6]	CM	Ice	Glycerol/water	Rim = solid ledge; Measures pressure (p) in gap. Predicts (a) $Q_s \uparrow$ as $f \downarrow$ as $s \uparrow$ and $\eta \downarrow$. (b) P versus η plot goes through maximum at 2 dPas
Tsutsumi [7]	HM	Sn/Pb	Stearic acid	Slag infiltration occurs in both t_n and t_p but more in t_p —slag inflow occurs at end of t_n . $Q_s \uparrow$ as $V_c \downarrow$, $\eta \downarrow$, $f \downarrow$, $s \uparrow$, $T_{sol} \downarrow$. Friction measured
Itoh [7], Nebeshima [7]	HM	Cu	Mould flux	Q_s dependent upon $(t_n + 0.5t_p)$. No η dependence for Q_s .
Kajitani [5]	CM	Moving polyester belt	Silicone oil	Mould = oscillating acrylic plate; Mould/ shell gap monitored. Gap profile is important. If gap narrows (as go downward) $Q_s \uparrow$ as $V_c \uparrow$, $\eta \uparrow$; if gap widens $Q_s \downarrow$ as $V_c \uparrow$, $\eta \uparrow$ suggests gap widens downward
Badri [9, 10]	M Sim	Steel	Mould slag	Oscillating mould. Principally focused on shell profile, heat flux and OM formation
Ko [11]	M Sim	Steel	Mould slag	Oscillating mould. focused on shell profile, heat flux and OM formation

CM cold model; HM hot model; M Sim mould simulator

- (b) *Hot models* use low-melting metals, like copper or tin, to represent the steel shell and the effects of changing variables are observed visually [7, 8].
- (c) *Miniature continuous casters* [9–11] are, bench-top versions of a continuous casting machine; they are fully instrumented to provide information about powder consumption, heat flux, friction, etc. The apparatus (see Sect. 3.2.4.2) consists of (i) a water-cooled copper mould which is inserted in a bath of steel covered with mould powder (the mould is in *inverse mode*, i.e. where the mould is surrounded by a slag film and a steel shell) (ii) an extraction system to provide continuous casting (iii) mould level control (iv) sinusoidal oscillation of the mould and (v) sensors to provide mould and steel temperatures, shell and mould displacements [9–11].

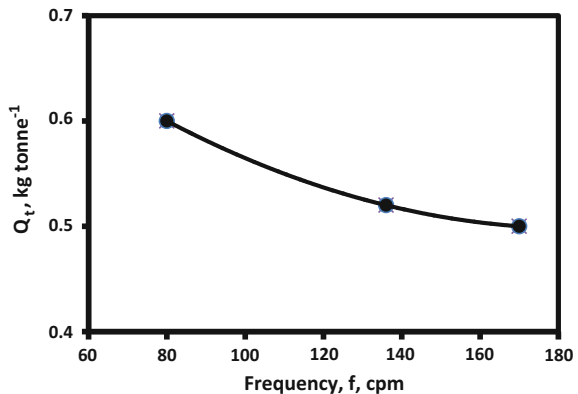
2.2.3.3 Mathematical Modelling Studies

The importance of the slag infiltration process is reflected in the number of mathematical models developed to predict the powder consumption; these models mostly make use of the Navier–Stokes equation [1, 13–25]. Billany et al. [26] and Gray [27] compared the predictions of the earlier models with plant data and observations. They found that:

- The models predicted the correct trends with casting speed, viscosity, etc.
- The models tended to slightly underestimate powder consumption.

However, one common problem with the model predictions is that they predict that Q_s increases with increasing frequency whereas most experimental data indicate the reverse relation, i.e. Q_s and Q_t decrease with increasing frequency (see Sect. 2.2.6.4) (Fig. 2.4).

Fig. 2.4 Powder consumption as a function of frequency [28] (permission granted ISIJ [28], re-drawn)



There are two approaches to modelling powder consumption. The first considers the powder consumption in its entirety. In the second approach, the various contributions to powder consumption are calculated individually [7, 19, 20] and collated. For instance, Meng and Thomas [19] consider that the powder consumption (Q_s) is made up of the following contributions:

- Liquid slag consumption (Q_l).
- Solid slag consumption (Q_{sol}) caused by any downward movement of the solid slag film.
- Powder consumption (Q_{OM}) caused by liquid slag trapped in the oscillation mark.

In some cases, $Q_{sol} + Q_l = Q_{lub}$ is assumed [7]. The powder consumption which is trapped in the oscillation mark (Q_{OM}) has been derived from calculations of the mean depth and the pitch of the oscillation mark [19] or from the relation, $Q_{OM} = 0.001f t_n \rho_l (t_n + 0.5t_p)$ [20].

Itoyama et al. [20] divided the powder consumption (Q_s) into the following contributions:

$$Q_s = Q_m + Q_g + Q_f + Q_{OM}. \quad (2.7)$$

where $Q_m (= \rho d_l^3/2)$ and $Q_g (= g \rho^2 d_l^3 / 12 \eta V_c)$ are associated with the pressure drop for parallel plates and the effect of gravity on the flow, respectively, Q_f is the flow associated with mould oscillation ($Q_f = (L_u/L_e) \rho s f L_e \sin(\beta/V_c)$) and $Q_{OM} = A_{OM} \rho f / V_c$ where β is the mould taper, L_e = effective length of mould) and L_u = relative, decreasing, distance when mould is ascending and A_{OM} = area of oscillation mark.

Saraswat et al. [4] calculated the values of Q_{OM} (denoted Q_{OM}^{calc}) and compared them with a database of powder consumption values recorded in different steel-works (Q_s^{total}). It was found that all of these models tended to seriously over-calculate Q_{OM} , i.e. $(Q_{OM}^{calc}/Q_s^{total}) > 1$ and frequently with values of 2 or more for this ratio.

Details of the various mathematical models are summarised briefly in Table 2.2.

2.2.3.4 Empirical Rules

A number of empirical equations have been deduced from analysis of plant data or from observations made in simulation tests. These are discussed in detail in Sect. 2.2.6. The equations and the effects of changes in the various factors are summarised in Table 2.3.

Table 2.2 Details of some published mathematical models covering slag infiltration

References	Model details	Comments, findings
Niggel [13]	Initially oscillation excluded. Assumes solid slag film adheres to mould; liquid moves down. Thermo-mechanical approach	Two regimes (i) $Q_{MR} \leq Q_{MR}^{req}$; (ii) $Q_{MR} \geq Q_{MR}^{req}$ Model predicts Q_s versus V_c exhibits a maximum
Schwerdtfeger [18]	Based on N-S eqn. for slag flowing between parallel plates. Needs data for d_{s+1} at meniscus and parallel plate regions Calculates velocity profile and P in gap	Shear stress and Friction calculated from velocity profile. Predicts shell bent away from mould during descent of mould and towards mould during ascent of the mould
Kor [14]	Based on N-S eqn. for slag flowing between two parallel plates— (1) moving at constant velocity and (2) oscillating	Must provide value of d_{s+1} and no account of thermal effects in the slag film
Hill [29]	Model to calculate slag flow, d_{-OM} : Max.vol flow rate, $Q_s^{max} = (2/3) \{ \eta / \Delta \rho g \}^{0.5} V^{1.5}$ N-S Eqn.	Predictions for d_{OM} : $d_{OM} \downarrow$ as $V_c \uparrow$ as $s \downarrow$ as $\eta \downarrow$
Nippon Steel [15, 16, 30]	Values of d_s and d_l not needed. Assumes mould oscillation affects viscosity. Rheological approach to calculate slag film thickness and velocity profile	Predicts (i) $d_l \uparrow$ as $\eta \uparrow$ and as $f \downarrow$ (ii) $Q_s \uparrow$ as $V_c \downarrow$ as $\eta \downarrow$ [26]. In agreement with plant data
Meng [19]	Couples transient slag flow model with solid slag stress and FD model of heat transfer. Uses Slag fracture and TTT data. Validated via Friction measurements on plant	Models used to check effects of V_c and η . F_1 gives negligible stresses. Slag film Fracture occurs near meniscus for crystalline and near mould exit for glass phase
Okazawa [17]	Uses Reynolds eqn, not N-S eqn. Steady state Unsteady state	Mould/shell gap widen as mould ascends; gap narrows during the ascent Gap opened during ascent and closed during descent of mould
Ojeda [22]	Couples, FF and HT. Values assumed for d_s , d_l ; men shape = Bickerman	Steel overflows at end of t_p . Rim exerts positive pressure. Positive Q_s during (t_n to early t_p) and negative Q_s during t_p . when V_m is high
Ramirez-Lopez [21]	Couples FF, HT and solidification. No assumptions re: d_s , d_l or men. shape	Follows Q_s , q , d_{shell} , d_s , d_l through osc.cycle, Q_s increases as mould/rim descends with max. in early t_p . Related to direction of flow in slag pool- downward-descending; outward-ascending
Jonayat [25]	Couples transient flow of metal and slag phases with heat transfer and solidification models Validated against plant data for Q_s	Parametric data: $Q_s \uparrow$ as $V_c \downarrow$, as $s \downarrow$ as $\alpha' \uparrow$ relation with f complex; $-Q$ ($\text{kg m}^{-1} \text{cycle}^{-1}$) \downarrow as $f \uparrow$
<i>FF</i> fluid flow in slag and metal; <i>HT</i> heat transfer; <i>men</i> meniscus; <i>osc</i> oscillation cycle; <i>N-S</i> Navier-Stokes; <i>P</i> pressure; Q_{MR}^{req} is required Q_s value; α' modification ratio		

Table 2.3 The predicted effect (increase ↑ or decrease, ↓) on Q_s with an increase in parameter (e.g. f)

References	Equation, Q_s	V_c	η	f	T_{sol}	T_{liq}	s	t_p	t_n	t_{cycle}	ρ_{slag}	d_l	d_{OM}
Wolf [62]	$Q_s = 0.1 + 0.55 (60/f\eta^{0.5} V_c)$	↓	↓										
Ogibayashi [42, 43]	$Q_s^{powd} = 0.60/\eta V_c$	↓	↓										
Wolf [41, 42], Fox [1]	$Q_s^{powd} = 0.70/\eta^{0.5} V_c$ $modified\ Q_s^{slag} = 0.55\eta^{0.5} V_c$	↓	↓										
Kwon [51]	$Q_s = 0.22 + 0.4\{60/(0.5\ s)^{0.3} f\eta^{0.5} V_c\}$	↓	↓	↓			↓						
Maeda [49]	$Q_s = 0.15\ f \cdot t_p/(\eta \cdot V_c)$	↓	↓	↑	↓			↑					
Nakajima [52]	$Q_s = 205400V_c^{-0.628} T_{liq}^{-0.866} t_p^{-0.341} f^{-0.076} \eta^{0.116}$	↓			↓		↑	↑		↓			
Sridhar [45]	$Q_s = 0.3/(\eta^{0.045} V_c)$	↓	↓										
Wolf 5 [63]	$Q_s = 0.5\ (s/f\eta\ V_c/1000)^{-0.5}$	↓	↓	↓			↓						
Jenkins [6]	$Q_s = (0.433\eta^{0.5})\ (1 + (0.0283\eta V_c))$	↓	↓										
Fox-modified [2]	$Q_s = (0.369\eta^{0.5})(1 + 0.1564\eta V_c^2) - 0.123$												
Nebeshima [7]	$Q_s = (\rho_1 d_{OM} d_s f 2 V_c) + (\rho d)$	↓		↑							↑	↑	↑
Tsutsumi [53, 64]	$Q_s = (k\beta s^{0.4} T_{sol}^{0.5} V_c) \cos^{-1} [1000V_c/2\pi f s]$	↓	↓	↓	↓		↑						
Emi [65]	$Q_l = 0.6\eta^{-0.15}$		↓										
Nakato [66, 67]	$Q_s = \rho_{slag}(0.143 - 0.003\eta)$		↓	↓							↑		
Kitagawa [57]	$Q_s = 0.0085\ t_p/f\ V_c$	↓		↑				↑					
Noguchi [68]	$Q_s = 10^{-3}(1952 - 246V_c - 44\eta - 1.07T_{liq})$	↓	↓		↓								
Kobayashi [69]	$Q_s = 0.003(t_{cycle} + t_p)^{1.5}/V_c$	↓	↓	↑				↑		↑			
Shimizu [70]	$Q_s = f t_p(0.0184(T_s - T_{liq}) - 2.58)/10V_c$	↓		↑				↑					
Itoyama [20]	$Q_s = Q_m + Q_g + Q_f + Q_{OM}$												
Shin [23]	$Q_s = [0.025\ \rho_1 k^{1.43} \{(2\Delta\gamma/\Delta\rho g)^{0.5} t_n^{0.556} \}^{0.389} \cdot v_s^{-1.49} + 0.507e^{3.59\eta}]\ (f/v_s)$ where $v_s = V_c 10^3/60$												
Saraswat [4]	$Q_s = e^{28.81} N_c f \eta^{-0.46} \cdot f^{0.49} \cdot s^{1.37} \cdot T_{br}^{3.48}$	↓	↓	↓	↓		↓						

when casting a LC steel where f : frequency; s : stroke; t_n : negative strip time; t_p : positive strip time; Q_m , Q_r , Q_g , Q_s defined in Sect. 2.2.3.1 (iii); P : analysis of plant trial data; Sim : simulation exp'ts; StA : statistical analysis of plant data

2.2.4 Problems Arising from Poor Powder Consumption

Inadequate powder consumption has been reported to cause:

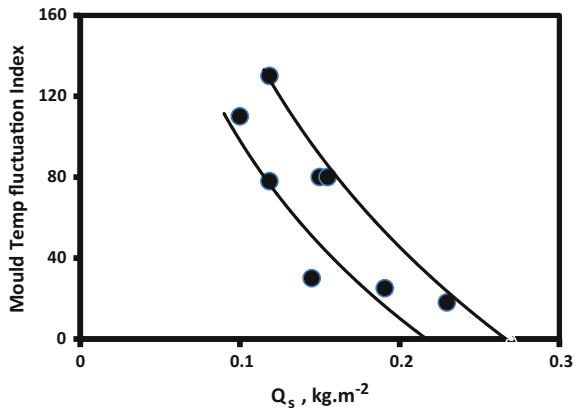
- Longitudinal cracking [31].
- Sticker breakouts (which are associated with a thin shell and poor lubrication).
- Deep oscillation marks [32, 33].
- Transverse cracking [34].
- Off-corner cracking [35, 36].
- The formation of depressions (when poor mould level control leads to the capture of the slag rim and the simultaneous cutting off of slag infiltration) [37–39].

Furthermore, heat flux (or mould temperature) variations were found to increase with decreasing powder consumption (Fig. 2.5) [40]. One of the principal causes of heat flux variations is the creation of a corrugated shell which is prevalent when casting peritectic, MC steels. The powders used to cast these steels are designed to give a thick, crystalline slag film to reduce the horizontal heat transfer. This is achieved by increasing T_{br} for the slag. However, a high T_{br} slag tends to create in a thin liquid slag film (d_l) which results in a low Q_s value. Corrugated shells are less common in other steel grades and so slags tend to have lower T_{br} values and hence higher Q_s values. Thus mould temperature fluctuations tend to exhibit an inverse relation with powder consumption (Fig. 2.5).

2.2.5 Optimum Casting Conditions

Wolf [41, 42] proposed that there was an optimum range for casting (i.e. the minimum friction and the optimum horizontal heat flux) which was defined in terms of the parameter (ηV_c^2) . This is shown in Fig. 2.6. The optimum conditions were found to occur when $(\eta V_c^2) = 5 \pm 3 \text{ dPas (m min}^{-1})^2$.

Fig. 2.5 Fluctuations in mould temperature as a function of powder consumption when using different casting powders (permission granted, ISS/AIST, [40])



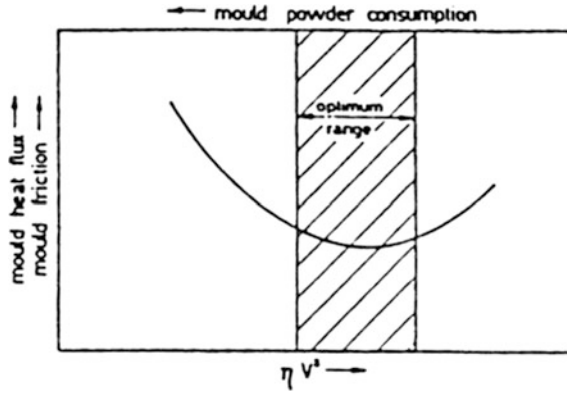


Fig. 2.6 Schematic drawing showing mould friction and horizontal heat flux as function of the parameter (ηV_c^2) (permission granted, VDEh/Stahl Eisen, [41, 42])

Ogibayashi et al. [43] reported that *fluctuations* in molten slag infiltration and mould temperature (heat flux) were at a minimum when the parameter, ηV_c , had a value in the range $1\text{--}3 \text{ dPas m min}^{-1}$ (Fig. 2.7a, b). A similar figure, involving fluctuations in the frictional force, also exhibits a minimum in this region (Fig. 2.7c) [44]. Thus the minimum fluctuations (i.e. optimum casting) occurs when $\eta V_c = 2 \pm 1 \text{ dPas m min}^{-1}$.

It can be seen from Figs. 2.5 and 2.6 that the equations, $\eta V_c^2 = 5 \pm 3 \text{ dPas (m min}^{-1})^2$ and $\eta V_c = 2 \pm 1 \text{ dPas (m min}^{-1})$ that powder consumption increases with decreasing viscosity. A plot of the viscosity of the casting slag as a function of the casting speed for mould fluxes used in a large number of steel plants revealed that the bulk of the data fell between the curves representing the Wolf [42] and Ogibayashi [43, 44] relations (Fig. 2.8 [45]). The outliers in the figure all relate to high-viscosity powders used in high-speed billet casting and this behaviour will be discussed in Sect. 2.2.6.10.

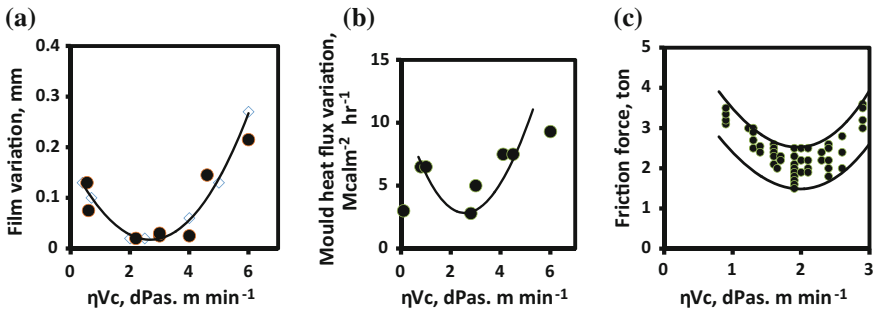


Fig. 2.7 Fluctuations in **a** Liquid slag film thickness on broad face (d_f) [43] **b** mould heat transfer (i.e., horizontal heat flux) [43] and **c** frictional force [44] as functions of the parameter, ηV_c (permission granted **a, b** Nippon Steel Sumitomo Metal Corp. [43] and **c** ISIJ [44])

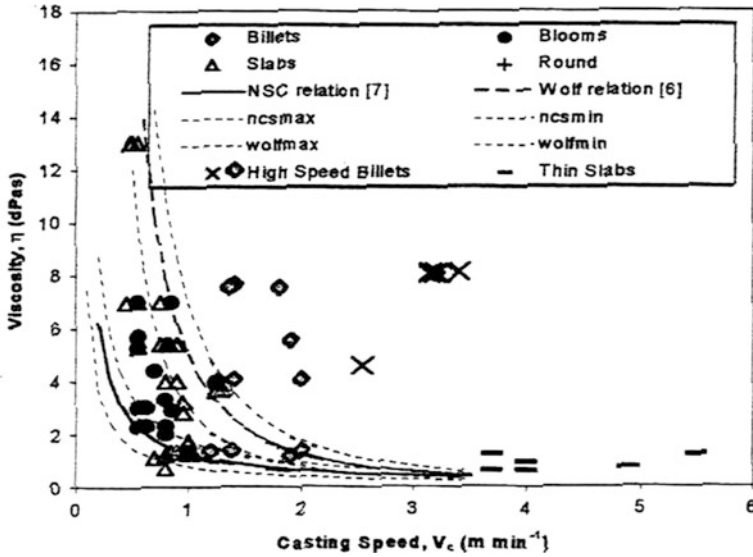


Fig. 2.8 Viscosity of mould slag at 1300 °C as a function of casting speed used in casting at a number of steel plants [45]; *dashed line* Wolf relation ($\eta V_c^2 = 5 \pm 3 \text{ dPas (m min}^{-1})^2$); *solid line* Ogibayashi relation, ($\eta V_c = 2 \pm 1 \text{ dPas (m min}^{-1})$); *dotted lines* bounds of above relations; Δ = slabs; — = thin slabs; o = blooms; \diamond = billets; + = rounds; X, \diamond = high-speed billets (permission granted, UNESID, [45])

2.2.6 Factors Affecting Powder Consumption

There are a number of factors affecting powder consumption, these are outlined below. These factors can be classified as following: (i) casting conditions, (ii) characteristics of the mould powders and slags and (iii) conditions arising from process problems.

2.2.6.1 Mould Dimensions

It was noted above in Eq. 2.1 that the frictional force increased as the surface area of the mould increased. Neumann et al. [46] proposed the powder consumption (Q_s) could be represented as function of the parameter, R^* (Fig. 2.9a, Eq. 2.8). This term represents the ratio of the (surface area/volume) for the mould. Alternatively, it can be regarded as the ratio of (the surface area of shell/volume of steel in the mould). It can be calculated from Eq. 2.9 where w and t are the width and thickness of the mould. The parameter, R^* , was used in Eq. 2.4 to calculate Q_s^{slag} from Q_t^{powd} .

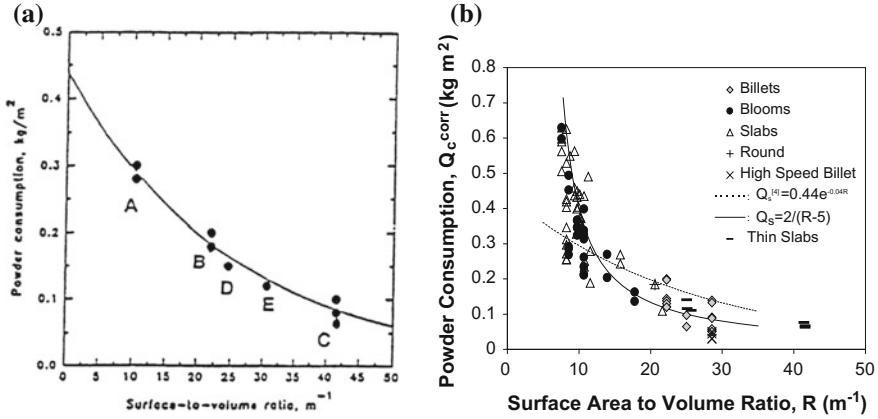


Fig. 2.9 Powder consumption, Q_s , as a function of the parameter, R^* **a** used in moulds with different dimensions; ($w \times t$ in m) A (1.5×0.22) B (1.0×0.1); C (1.3×0.050); D (0.16×0.16); E (0.13×0.13) [46] and **b** \diamond = billets; \circ = blooms; Δ = slabs; — = thin slabs; $+$ = Rounds; \times = high-speed billets; dotted line = Eq. 2.8 [46]; solid line = ($Q_s = 2/(R - 5)$) [45, 47] (permission granted), ISS/AIST, [46] and **b** UNESID, [45]

$$Q_s = 0.44 \exp^{-0.44R^*} \quad (2.8)$$

$$R^* = 2(w + t)/w \cdot t \quad (2.9)$$

Subsequently, a similar study based on a much larger database and found that the data shown in Fig. 2.9b could be represented better by Eq. 2.10 [45, 47].

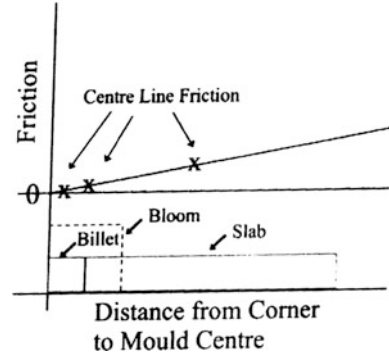
$$Q_s (\text{kg m}^{-2}) = 2/(R^* - 5) \quad (2.10)$$

Typical R^* values are for Slabs 9–15; for Blooms 10–18; for Billets 22–30, Thin slabs 40. It can be seen from Fig. 2.9b that the *required* powder consumption is much greater for slabs than that for billets. Ogibayashi [34] pointed out that frictional forces on the broad face tended to increase as the distance from the corner increased. Consequently, Fox [2] derived an alternative relation for powder consumption, ($Q_t f^*$), in terms of distance from the corner, D_{com} (Fig. 2.10 and Eq. 2.11.); note ($Q_t f^*$) was calculated to avoid using R^* in the conversion of Q_t^{powd} to Q_s^{slag} .

$$(Q_t f^*) = 0.615 D_{\text{com}}^{0.586} \quad (2.11)$$

The overall conclusion is that mould dimensions have a marked influence on the required powder consumption, regardless of whether the parameters R^* or D_{com} is used. However, with thin slabs the high value of R^* suggests thin slabs require little powder consumption whereas the fact the D_{com} is quite large suggests that a high powder consumption is needed. It is also true that powder consumption values tend to be low in thin-slab casting. The shell in thin-slab casting tends to be very thin

Fig. 2.10 Schematic diagram showing friction increasing with increasing distance of corner to centre; X = friction at *centre line* for 3 mould geometries; *solid line* = billet; *dotted line* = bloom and *solid line* = slab; (courtesy of AB Fox [2])



because of the short residence time in the mould and thus shell shrinkage and the size of the gap tend to be low also. Some support for this view is that 400 mm thick slabs at Dillinger (where the shrinkage is high) tend to have high powder consumption (Figs. 2.9b and 2.10).

2.2.6.2 Effect of Casting Speed

The effect of casting speed on powder consumption has been investigated by a large number of workers [1, 3, 4, 20, 21, 23, 25, 32, 42, 46–52].

In Sect. 1.4 above, it was pointed out that Wolf [41, 42] proposed that optimum casting was obtained when $\eta V_c^2 = 5 \pm 3 \text{ dPas (m min}^{-1})^2$ and that Ogibayashi et al. [43] found the fluctuations were at a minimum, (for both slag film thickness and heat flux) when $\eta V_c = 2 \pm 1 \text{ dPas (m min}^{-1})$. Subsequently, Wolf [42] converted these relations into optimum powder consumption equations, i.e. Eqs. 2.12 and 2.13, respectively.

Wolf:

$$Q_{\text{sreq}}^{\text{powd}} = 0.7/\eta^{0.5} \cdot V_c \quad (2.12)$$

Ogibayashi:

$$Q_{\text{sreq}}^{\text{powd}} = 0.6/\eta \cdot V_c \quad (2.13)$$

An investigation using a much larger database of Q_s values, subsequently indicated a modified version of Eq. 2.12 (given in Eq. 2.14) provided a better fit with plant data [1, 48].

$$Q_{\text{sreq}}^{\text{slag}} = 0.55/\eta^{0.5} \cdot V_c \quad (2.14)$$

These equations all indicate that powder consumption decreases as the casting speed increases.

2.2.6.3 Slag Viscosity

The effect of viscosity on powder consumption has been studied by a number of investigators [1, 15, 20, 21, 25, 31–33, 38, 45, 49–54].

It can be seen from Eqs. 2.12 to 2.14 that powder consumption increases with decreasing viscosity. The powder consumption values obtained on plant with high-viscosity fluxes used in high-speed billet casting are significantly lower than *required* Q_s values calculated with Eqs. 2.12–2.14. This is discussed in Sect. 2.2.6.10. Low consumption values are also recorded on plants casting Ti-stabilised stainless and LC steels. This is thought to be due to the blocking off of slag infiltration by accretions of Ti(CN) or *perovskite* ($\text{CaO} \cdot \text{TiO}_2$) at the mouth of the shell/mould channel (see Sect. 2.2.6.9). The minimum powder consumption providing acceptable levels of lubrication has been discussed [42]. Recommended values of Q_s for casting sticker sensitive steel grade are 0.3 and 0.4 kg m^{-2} for round billets and HC steel grades, and for crack-sensitive grades, values of 0.25 and 0.4 for round billets and heavy plate, respectively [42]. For high-speed casting, minimum values of $Q_s = 0.1 \text{ kg m}^{-2}$ have been recommended [55]. The minimum levels of powder consumption required to avoid solid friction (which causes fracture of the slag film) has also been discussed [19].

Values of Q_s for non-Newtonian mould slags have been compared with those for conventional slags ($Q_s \text{ } c_{\text{onv}} < Q_s \text{ non-Newt}$) since the high shear forces in the infiltration region result in a reduction of their viscosity [56].

2.2.6.4 Oscillation Parameters

The effects of the various oscillation parameters have been investigated by a number of workers [1, 4, 20, 21, 23, 31, 32, 42, 49, 51–53, 57–61]. Various equations have been reported for the calculation of powder consumption; these involve a number of variables (e.g. casting speed, frequency, etc.). A number of the reported equations are given in Table 2.3; the effect of an increase in the variable on the powder consumption is also given. Inspection of Table 2.3 indicates:

- There is reasonable agreement that increases in casting speed, viscosity and break temperature (T_{br}) all result in a decrease in powder consumption.
- There is little agreement on the effect of other variables controlling powder consumption
- There is no agreement on the effects of the oscillation characteristics; it should be pointed out that some workers considered slag infiltration to occur during negative strip time t_n , (i.e. when the mould is descending faster than the shell) which results in increased pressure produced by a descending slag rim. In the other school of thought, slag inflow is considered to be difficult in t_n (since the channel gets blocked by the bending of the shell in this period) and thus slag infiltration largely occurs in positive strip time, t_p , (where $t_p + t_n = t_{\text{cycle}}$). It has been reported that Q_s exhibited a stronger correlation with t_p than with t_n [25].

- Some of the experimental studies indicate that Q_s decreases with increasing frequency (Fig. 2.4) but as can be seen from Table 2.3 other studies show the reverse relation with frequency (i.e. $Q_s \uparrow$ as $f \uparrow$)
- Wolf [42] examined plant data where all casting variables were kept constant except the stroke length which was altered (i.e. t_n and t_p will change) and found that as the stroke increased Q_s increased ($Q_s \uparrow$ as $s \uparrow$) as shown in Fig. 2.11. This is supported by plant data from Oxelösund Steelworks which exhibited a strong relationship between stroke length and mould powder consumption. However, a statistical analysis of plant data showed the reverse trend ($Q_s \uparrow$ as $s \downarrow$) and a parametric study suggested that increasing stroke only had a slight effect on Q_s [25].

2.2.6.5 Non-sinusoidal Oscillation

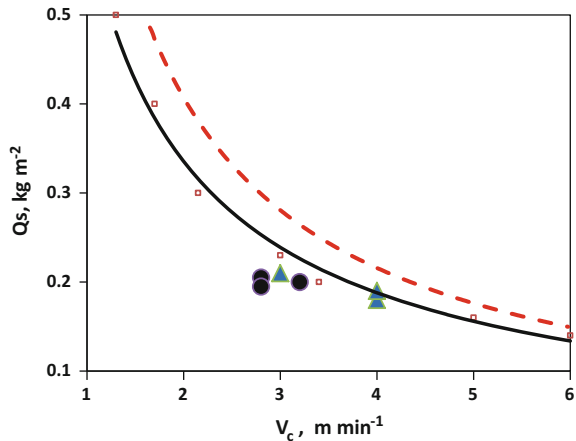
Several workers have reported that non-sinusoidal oscillation increases powder consumption [25, 49, 53, 60, 64, 71]. It can be seen from Fig. 2.12 that the use of non-sinusoidal oscillation leads to a 10% increase in powder consumption.

2.2.6.6 Solidification (or Break) Temperature (T_{br})

The effect of break (or solidification) temperature on powder consumption has been studied by a number of investigators [4, 16, 20, 51–53, 64].

It can be seen from Table 2.1 that those equations which involve T_{br} (or T_{sol} , or T_{liq}) all agree that an increase in T_{br} results in a decrease in powder consumption ($Q_s \downarrow$). This can be seen in Fig. 2.13. This is consistent with intuition since it can be

Fig. 2.11 Powder consumption as a function of casting speed showing Q_s increasing with increasing stroke length; ---, $s = 8$ mm; — = 6 mm; •, ▲ = experimental data (permission granted, VDEh/Stahl Eisen, [42])



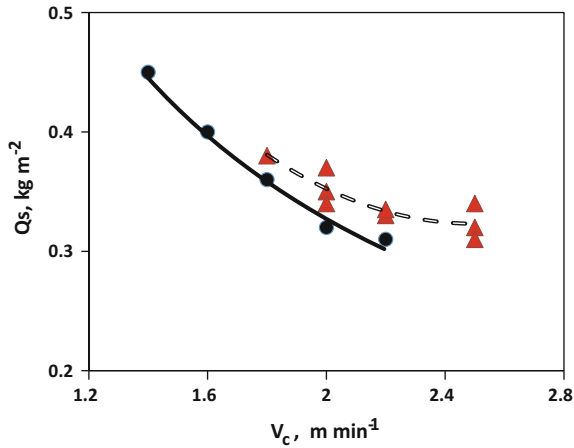
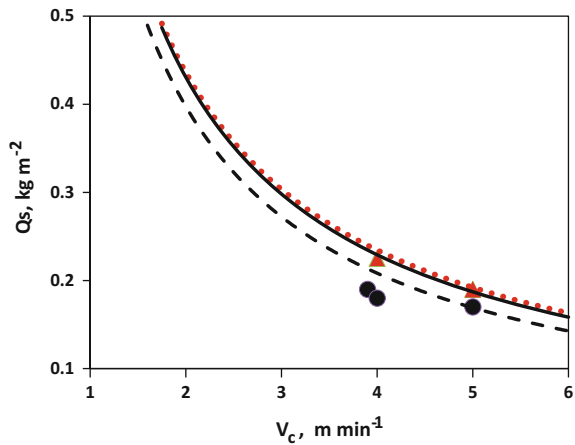


Fig. 2.12 Powder consumption as a function of casting speed showing non-sinusoidal oscillation --▲-- provides a 10% higher Q_s than sinusoidal oscillation (—●—) (permission granted, ISIJ, [49])

Fig. 2.13 Powder consumption, Q_s , as a function of casting speed showing Q_s decreasing as T_{sol} or T_{br} increases as T_{sol} or T_{br} increases; ▲, ● = experimental values; T_{br} : ••• = 952 °C; — = 970 °C, - - - = 1027 °C; (permission granted, VDEh/ Stahl Eisen, [42], re-drawn)



seen from Fig. 2.14 that an increase in T_{br} leads to a decrease in thickness of the liquid film ($d_l \downarrow$) and an increase in solid film thickness ($d_s \uparrow$).

The mathematical model reported by Ramirez-Lopez [1, 21, 54] indicated that the horizontal heat flux increased gradually in the period of the oscillation cycle where the mould was descending. The increased heat flux, in turn, caused solid slag to melt, resulting in an increase in liquid film thickness ($d_l \uparrow$) and a decrease in the solid film thickness ($d_s \downarrow$). This process was reversed when the mould ascended. Thus, the liquid layer increased at the expense of the solid layer when the heat flux was increasing and *vice versa* when the heat flux was decreasing.

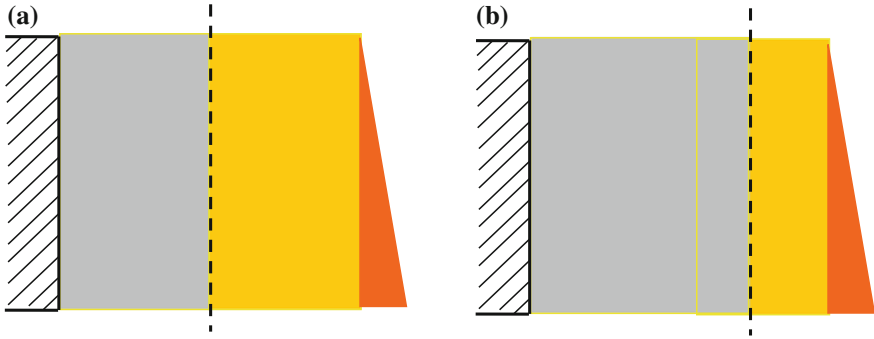


Fig. 2.14 Schematic drawing showing effect of increasing T_{br} on the thicknesses of solid and liquid films, where $T_{br(b)} > T_{br(a)}$ (note relative thickness values are not to scale)

2.2.6.7 Melting Rate

It was pointed out in Sect. 2.2.1 that powder consumption (in kg min^{-1} or kg s^{-1}) in Eq. 2.5 (Q_{MR}^{slag}) can be viewed as the melting rate. The powder consumption has been found to increase with increasing slag pool depth (d_{pool}) [72] and d_{pool} is affected by the melting rate. In practice, the melting rate is controlled by the amount of free carbon and, to a lesser extent, by the size of the carbon particles (see Sect. 4.3). Consequently, it is important that powder consumption is close to the *required* Q_s for the given casting conditions (mould dimensions, casting speed, etc.), i.e. it is not restricted by an excessively high carbon content of the mould powder. A few casting powders have a carbon content which is too high and thus leads to a restricted slag infiltration.

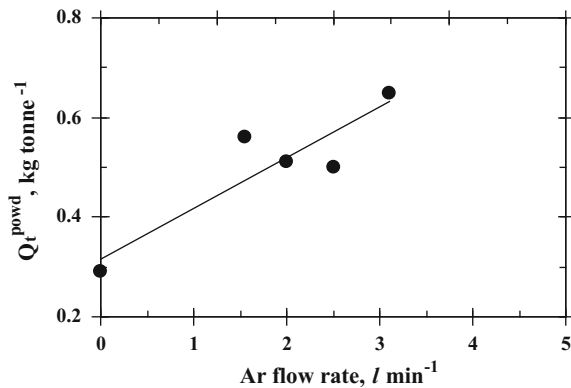
2.2.6.8 Superheat (ΔT)

The effect of superheat on powder consumption has been studied by several investigators [1, 3, 16]. Increasing superheat results in increased powder consumption. On the basis of Eq. 2.12 or Eq. 2.13 increases in superheat will lead, sequentially, to an increase in slag temperature, a lower viscosity and a higher value of Q_s .

2.2.6.9 Argon Flow

It has been reported that powder consumption increases with increasing argon flow rate [73] (Fig. 2.15). One possible reason for this behaviour is that an increased Ar flow rate causes more convection and hence, a higher vertical heat flux which, in turn, increases the melting rate. A high Ar flow rate is known to affect the metal flow patterns in the mould.

Fig. 2.15 Plant measurements of powder consumption, Q_t , as a function of Ar flow rate; (courtesy of Fox [2])



2.2.6.10 Continuous Casting of Steels Containing Ti

It has been observed that powder consumption is frequently lower than predicted when casting steel grades containing Ti. This is thought to be due to the formation of TiN or Ti(C, N) which has a low solubility in the slag pool and thus, tends to exist as solid particles [74, 75]. These particles agglomerate through turbulent collisions and the agglomerates restrict the slag flow when they are sited in the mouth of slag/mould channel (Fig. 2.16) [74, 76]. The solid particles also increase the slag viscosity and thus, decrease Q_s . Alternatively, TiO_2 particles can form *perovskite* ($\text{CaO} \cdot \text{TiO}_2$) which has a high melting temperature and thus reduces both the thickness of the liquid slag film (d_l) and Q_s . It is necessary to keep the basicity, $(\text{C/S}) < 1.0$ to avoid *perovskite* formation [77].

2.2.6.11 High-Viscosity Powders

The powder consumption data for most powders follow the empirical rules based on the viscosity and casting speed [2, 42, 43] the only exceptions are the high-viscosity ($\eta_{1300} = 10\text{--}30$ dPas) powders used for high-speed billet casting [2] and those used in casting steel grades containing Ti. In high-speed billet casting, considerable turbulence is generated which results in significant levels of slag entrapment. One way of reducing slag entrapment is to increase the slag viscosity. However, the reduction in slag entrapment levels comes at the expense of a significant decrease in powder consumption. Fortunately, the powder consumption required for billets is low (since the distance from centre line to corner is low and, furthermore, R^* has values > 22) which means this practice is widely used to minimise slag entrapment.

It has been suggested that these high-viscosity slags will form super-cooled liquids (*scl*) rather than crystallites during cooling. The *scl*, although viscous, will move in response to any stress applied by the ferro static pressure, the downward movement of the shell or the oscillating motion of the mould; hence, the slag (*scl*)

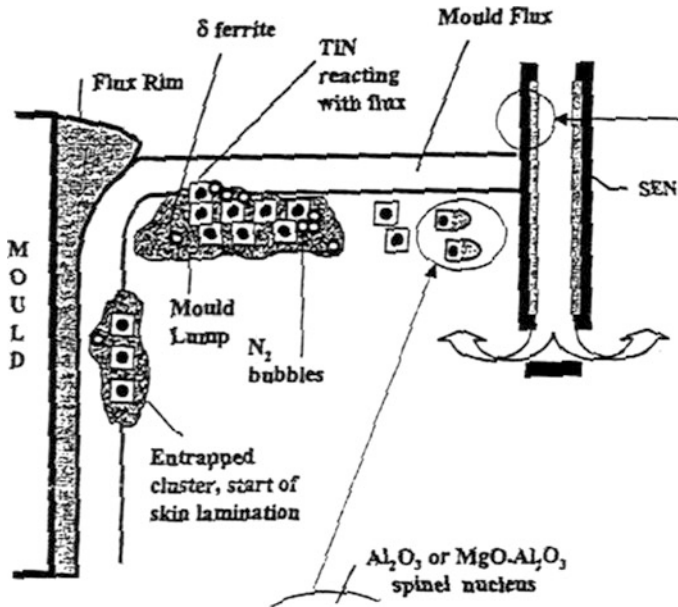


Fig. 2.16 Schematic drawing showing formation of agglomerates of Ti(C, N) when casting steels containing Ti; (permission granted, ISS/AIST [74])

will supply some lubrication to the shell. The importance of retaining some glass phase in the slag film has been pointed out by Hanao et al. [78].

2.2.6.12 Electromagnetic Braking (EMBr) and Casting (EMC)

Electromagnetic devices are reported to increase powder consumption. The application of electromagnetic braking (EMBr) results in a 30% decrease in vertical heat transfer [79] from the steel, resulting in a *ca.* 10 °C increase in meniscus temperature [80–83]. This increased meniscus temperature results in a lower slag viscosity and higher powder consumption. EMBr is widely used in high-speed, thin-slab casting where powder consumption tends to be low [84].

Increases of 20% in Q_s , have been reported when using pulsative, Electromagnetic casting (EMC) [85]; it is known that the pinch force in EMC reduces the horizontal heat transfer, which, in turn, results in increases in both meniscus temperature and Q_s .

2.2.6.13 Liquid Slag Feeding to the Mould

Some high Al-and Mn-steels have low-melting temperatures, so the vertical heat flux is insufficient to melt the mould powder. Consequently, liquid slag feeding technology has been developed to provide liquid slag to the steel surface. It is reported that powder consumption is increased with liquid slag feeding [86].

2.3 Slag Infiltration During the Oscillation Cycle

A number of empirical rules have been proposed to calculate the powder consumption. These are given in Table 2.3 and are based on plant observations and physical modelling results. It was mentioned above that there is general agreement that the powder consumption increases as the casting speed (V_c), slag viscosity (η) and break temperature (T_{br}) all decrease. However, there is no consensus as to (i) which of the various oscillation parameters affect Q_s or (ii) the way in which they affect Q_s . Furthermore, there are two schools of thought concerning the period of the oscillation cycle where slag infiltration occurs;

- The first identifies t_n as the primary period of slag infiltration, where the descending slag rim increases the pressure on the molten slag which responds by infiltrating into the shell/mould channel and
- The second considers t_p as the principal period of infiltration, since infiltration is restricted in t_n because the bending-back of the shell is considered to block off the slag flow during this period; thus slag infiltration is restricted to t_p where the shell does not interfere with the infiltration.

The infiltration mechanism has been studied in (i) plant trials [3, 55, 87–89] (ii) cold modelling studies [5, 6, 12, 58, 90] (iii) hot modelling studies [7, 53, 91] and (iv) mathematical modelling of the heat and fluid flow [1, 12, 16, 21, 22, 25, 36, 92, 93].

Mathematical models based on Navier–Stokes equations do provide a reasonable description of the effects of casting speed, slag viscosity and T_{br} , but, for the most part, they also predict that Q_s increases with increasing frequency which disagrees with most experimental observations, e.g. Fig. 2.4. In an attempt to explain these discrepancies, mathematical models have been developed to explore in which part of the oscillation cycle the slag infiltration takes place [1, 21, 22, 25, 54].

It is customary to characterise oscillation in terms of negative and positive strip times (t_n and t_p , respectively) where t_n represents the time when the mould is descending faster than the shell and t_p constitutes the remainder of the cycle (i.e. $t_n + t_p = t_{\text{cycle}} = 60/f$ where f is in cpm). However, the oscillation cycle can also be characterised in terms of the position of the mould. The mould and the slag rim will be at their highest position in late t_p (denoted t_p^{late}). It descends throughout t_n and reaches its lowest position in early t_p (t_p^{early}). The mould will then ascend steadily through t_p .

The findings of the two studies due to Ojeda [22] and Ramirez–Lopez [1, 21, 54] are in good agreement with both proposing that slag infiltration occurs during the descent of the mould/rim covering the period ($t_n - t_p^{\text{early}}$) and that there is little slag infiltration during the ascent of the mould (in t_p). This can be seen in Fig. 2.17c and it was also noted that the rate of slag flow into the shell/ mould channel is at its highest when the mould/slag rim was at its lowest position (i.e. between t_n^{late} and t_p^{early}).

The directions of flow in the slag pool at different periods of the oscillation cycle have also been studied in the several investigations [1, 21, 22, 54] and are shown in Fig. 2.18. It can be seen when the mould and slag rim are at their highest position (Fig. 2.18a) that the slag flow into the mouth of the channel is radially outward and upward. As the mould/rim descends the slag direction changes to downward and there is evidence of a vortex in the region of the mouth (Fig. 2.18b). When the mould and slag rim reach their lowest positions (in t_p^{early}) the flow is strongly downward into the channel (Fig. 2.18c). Finally, halfway through t_p the flow changes direction to radially—outward and upward (Fig. 2.18d). Thus the direction of the flow in the slag pool plays a significant role in the slag infiltration into the shell/ mould channel and this is affected by the direction of movement of the mould and slag rim.

The slag rim acts like a piston and helps to inject slag into the channel. However, the movement of the mould alone will cause some downward flow of slag but the slag rim certainly accentuates the downward slag flow.

Just after the mould reaches its highest position there is a *tide—change* in the slag flow (radially outward and upward to downward) which results in a period of “*confused flow*” (the remnants of which are shown in Fig. 2.18b). There is a similar period of confused flow after the mould and rim reach their lowest points. There is very little slag infiltration during these periods of confused flow. It has been suggested that the lack of slag infiltration in the periods following a tide-change is responsible for the failure of the models based on the Navier–Stokes equation to predict the correct Q_s dependency on frequency (namely, $Q_s \downarrow$ as $f \uparrow$) observed on plant [1]. For example, if $f = 60$ cpm and is increased to 120 cpm, there will twice as many tide-changes per unit time. Since little powder consumption occurs during these tide-changes, the increased number of tide-changes per minute will result in an overall decrease in Q_s . A parametric study showed [25] indicated that a 60% increase in frequency resulted in only 2% change in Q_s (where both increases and decreases in Q_s were recorded for different stroke lengths). However, it was found Q_{cycle} ($\text{kg m}^{-1} \text{cycle}^{-1}$) decreased by 35% with a 60% increase in f .

In summary, slag infiltration occurs through the downward flow of slag resulting from the downward movement of the mould; the slag rim accentuates this slag flow. The size of the slag rim is dependent upon the steel grade being cast, with high basicity (C/S) slags (used for MC steels) forming large rims and low-(C/S) slags forming smaller rims (see Fig. 1.4).

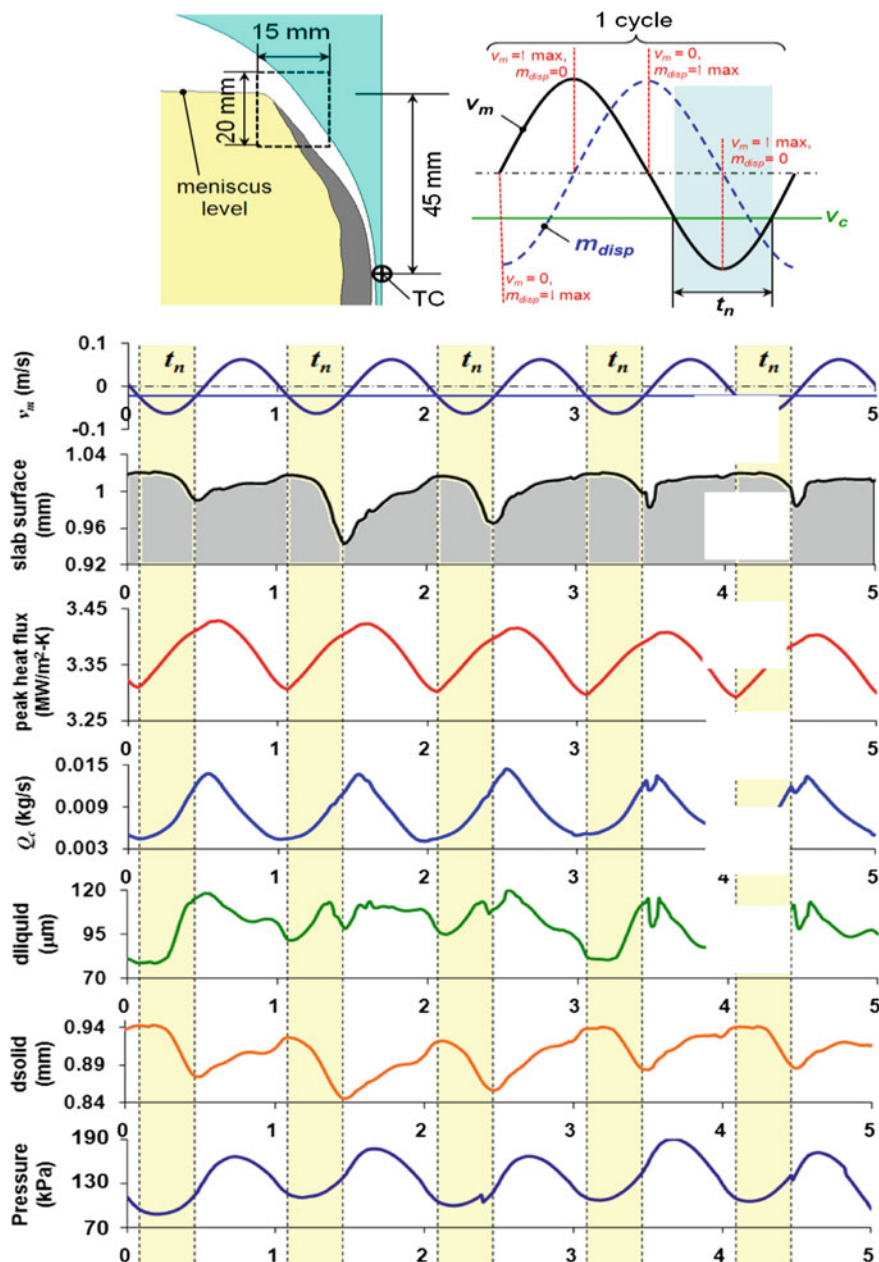


Fig. 2.17 Mathematical model predictions of **a** profile of strand surface, **b** heat flux, **c** powder consumption in kg s^{-1} , **d** liquid film thickness d_l , **e** solid slag film thickness, d_s and **f** pressure during five oscillation cycles [1, 21, 54] the dotted, vertical lines indicate the onset (left) and end (right) of negative strip periods of each cycle (0–5). Note that peaks in Q and d_l lie in early t_p ; (permission granted, ISIJ, [21])

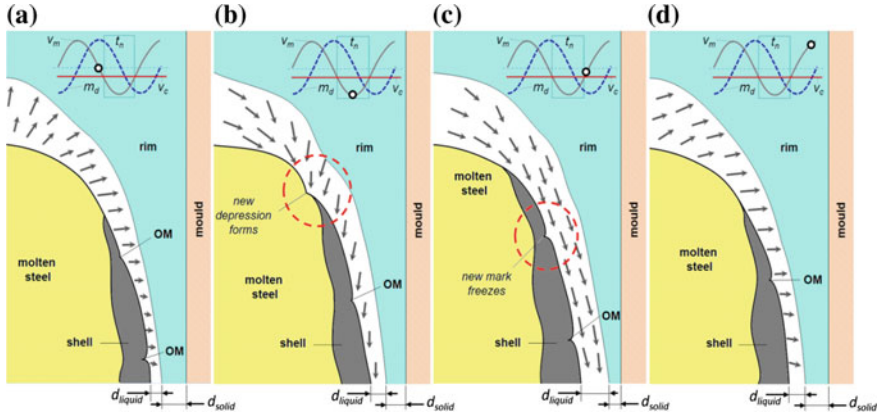


Fig. 2.18 Schematic diagram showing the direction of slag flow at different parts of the oscillation cycle **a** at highest position of mould in late t_p , **b** halfway through t_n , **c** at lowest position of mould in early t_p and **d** midway through t_p [1, 21, 54] (permission granted, ISIJ, [21])

2.4 Empirical Equations for Calculating Powder Consumption

A number of empirical rules have been proposed to calculate the powder consumption; the proposed equations are given in Table 2.3. Fox [2] carried out an evaluation of the various empirical equations. This evaluation compared predictions with plant measurements contained in an extensive database of powder consumption and casting variables for a large number of trials carried out at different steelworks casting slabs, blooms, billets and thin slabs. It should be pointed out that the database contained powder consumption for high-viscosity billet powders used to minimise slag entrapment at high casting speeds; Q_s data for these slags are much lower than for other powders and tend to distort the fit. The performance was judged from Δ_{RMS} which is calculated from Eqs. 2.15 and 2.16 where N = the number of mould slags. The best performing models for this database were found to be in the hierarchy, Ogibayashi [42, 43] > Kobayashi [69] > modified Wolf [1, 2] > Maeda [49]

$$\delta = 100(Q_{\text{meas}} - Q_{\text{pred}})/Q_{\text{meas}} \quad (2.15)$$

$$\Delta_{\text{RMS}} = \{\sum(\delta_1^2 + \delta_2^2 + \delta_3^2 + \dots)\}^{0.5}/N \quad (2.16)$$

Analysis of plant data for powder consumption for slab-, bloom- and billet-casting indicated that $Q_t^{\text{slag}} (= f^* \cdot Q_t^{\text{powd}})$ is reasonably constant at $0.48 \text{ kg (tonne steel)}^{-1}$ except for the “high-viscosity billet powders” mentioned above in Sect. 2.2.6.10.

2.4.1 Frictional Forces

Frictional forces (F) acting on the shell contain contributions from the liquid frictional (F_l) and solid frictional (F_s) forces (Eq. 2.17).

$$F = F_l + F_s \quad (2.17)$$

It was pointed out in Eq. 2.1 that the liquid frictional force was inversely, dependent on the thickness of the liquid layer (d_l). Since $d_l = (Q_s/\rho_l)$ Eq. 2.1 can be re-written as

$$F_l = A \cdot \eta(V_m - V_c)\rho_l/Q_s. \quad (2.18)$$

It can be seen that the liquid friction force is inversely dependent upon the powder consumption and directly related to the slag viscosity and the difference between the velocities of the mould and the strand.

The frictional forces tend to be highest when casting MC steels because the corrugated shell formed increases both A and F_l and d_l tends to low because high T_{br} slags are used to cast these steels. The friction forces measured when casting with mould powders are lower than those for oil casting [94]. Longitudinal cracking has been correlated with high frictional forces [95]. Frictional forces tend to decrease as the cast proceeds [95].

Solid friction (between the shell and the solid slag) tends to occur in the lower half of the mould. The formation of *star and spongy cracks* (Sect. 11.7) is associated with solid/solid friction and the consequent *spalling* of the solid slag film which can even result in the pick-up of copper by the strand. However, solid friction may also occur in the upper mould in the corner regions if the corners are overcooled [4].

Since solid friction can occur in the bottom of the mould it is important to ensure that all of the mould receives liquid lubrication [96]. A lubrication index (LI) was proposed by Billany et al. [96] which is a measure of the fraction of the mould enjoying liquid lubrication; this index is defined in Eq. 2.19. Ideally, the parameter, LI, should have a value of 1.0.

$$LI = (\text{Distance from meniscus to point where } T = T_{br}) / (\text{Distance} - \text{meniscus to mould exit}) \quad (2.19)$$

If solid friction is a problem in the lower half of the mould, probably the best measure is to increase the casting speed. In theory, a decrease in the flow rate of the cooling water would also be beneficial but in practice, the remedial effect is small.

Sorimachi et al. [97] have pointed out that:

- The frictional forces refer to the entire mould wall and not to the local frictional forces in the meniscus region which is of key importance in the formation of sticker breakouts.
- The measured friction is that acting on the mould wall and is not that acting on the shell.

2.4.1.1 Measurement of Frictional Forces

Measurements on frictional forces have been derived using plant trials, simulation experiments and mathematical modelling of the frictional forces.

Plant Measurements of Friction

In the past, a number of investigators have measured frictional forces by using load cells attached to the oscillating mechanism and then applying Fourier analysis of the signals produced [27, 71, 98]. Alternatively, frictional forces can be measured using the MLTEKTOR system [99]. These devices have been used for the detection of defects and longitudinal cracks [44, 100, 101].

Friction Measurements in Simulation Tests

Several tests have been devised to simulate the frictional forces acting on the shell when using different mould fluxes. Short descriptions of these tests are given below.

Rotating Cold Finger Test

In this test, a water-cooled, copper finger (representing the mould) is rotated in a steel crucible (representing the strand) containing the molten mould flux [98]. The copper finger becomes covered with a solid slag film of ca. 3 mm thickness and a thin liquid layer. The frictional forces are measured by determining the torque developed on the steel crucible as the finger is rotated at constant velocity (10–50 rpm). The apparatus is shown in Fig. 2.19a.

Oscillating Cold Finger Test

This test resembles the rotating cold finger test but the cold finger is oscillated vertically instead of being rotated [9, 11, 53, 102].

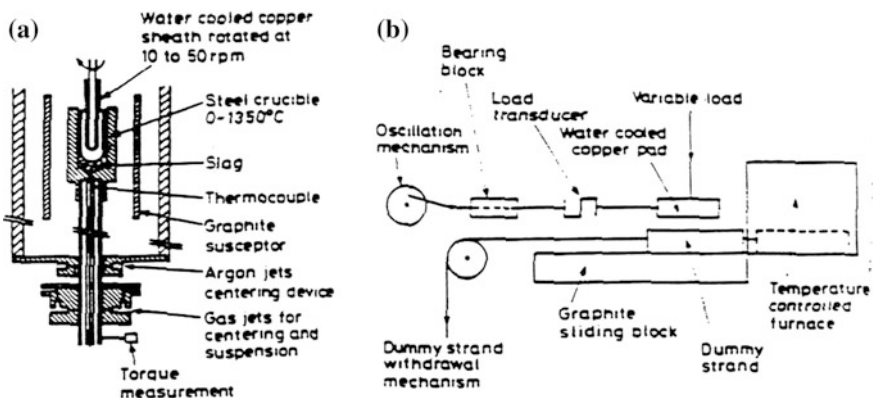


Fig. 2.19 Schematic drawings showing the apparatus used in **a** the rotating cold finger test [98] and **b** the oscillating pad method [27, 103] (permission granted, Europ. Comm. Sci. and Tech. Publ. [27])

Oscillating Pad Test

In these tests, a water-cooled copper pad (mould), which can be oscillated at different frequencies, is lowered onto a heated steel block (strand) covered with molten mould slag (Fig. 2.19b). The block is then withdrawn at a fixed speed and the frictional force exerted by the pad is measured as it bears down on the strand by using a load cell mounted on the oscillation arm. The thickness of the molten slag layer (ca. 0.3 mm) was monitored using a displacement transducer [27, 103].

Rotating and Oscillating Pads Test

A simulation test was reported by Sorimachi et al. [97] and is shown in Fig. 2.20. In this test a graphite disc (representing the strand) is rotated unidirectionally). A second, lower, graphite disc (representing the mould) contains a 2 mm deep liquid, mould slag of known viscosity; and this disc is oscillated sinusoidally. The torque is measured continuously.

Miniature Continuous Caster

Friction measurements have been carried out in a miniature continuous caster [91]. In order to view the solidification process of the shell the steel was replaced by Sn–5%Pb, the mould slag by stearic acid with Al_2O_3 particles to act as tracers and one side of the oscillating, 50 mm², Cu mould was replaced by silica to facilitate viewing [91]. The friction between mould and shell was measured by load cells sited

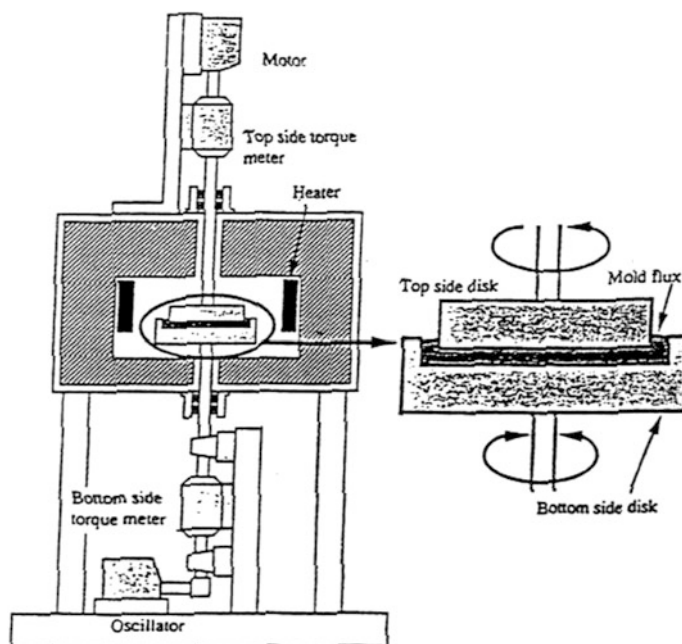


Fig. 2.20 Schematic drawing showing the apparatus used by Sorimachi et al. [97] (permission granted, ISS/AIST [97])

below the mould. The frictional force per unit area between mould and shell was taken as $\Delta F/A = (F_{\max} - F_{\min})/A$ where A = surface area and the subscripts max and min represent the maximum and minimum load in any one cycle, respectively. Values of $\Delta F/A$ were found to decrease as liquid film thickness (d_l) increased and $(V_m - V_c)/d_l$ decreased (i.e. $\Delta F/A \downarrow$ as $d_l \uparrow$ and as $\{(V_m - V_c)/d_l\} \downarrow$) [91]. Friction measurements can be made in a similar manner in mould simulators [9–11].

2.4.1.2 Mathematical Modelling of Friction in Mould

Mathematical modelling of the frictional forces in the mould has been reported [12, 18, 53, 97]. Schwerdtfeger and Tacke [18] derived a relation for the shear stress in the liquid slag based on computations of the velocity. The frictional force was calculated by multiplying the calculated stress by the area wetted by the slag.

2.4.2 Factors Affecting Frictional Forces in the Mould

It can be seen from Eq. 2.18 ($F_l = A\eta (V_m - V_c) \rho_l/Q_s$) that the liquid friction force (F_l) is inversely dependent upon the powder consumption (Q_s); thus it follows F_l will increase as Q_s decreases ($F_l \uparrow$ as $Q_s \downarrow$). However, Q_s is dependent upon other factors, e.g. casting speed; the effect of the various parameters are given below.

However, high friction measurements recorded on plant (i.e. 10–20 kPa) have been attributed to (i) movement of the solid slag layer (ii) excessive taper and (iii) mould misalignment [19]. At low casting speeds the critical consumption is high so variations in consumption, Q_s , can lead to slag film fracture and high, solid friction forces. In contrast, at high casting speeds the principal causes of high frictional forces are excessive taper (see Fig. 1.48) and mould misalignment [19].

2.4.2.1 Casting Speed (V_c)

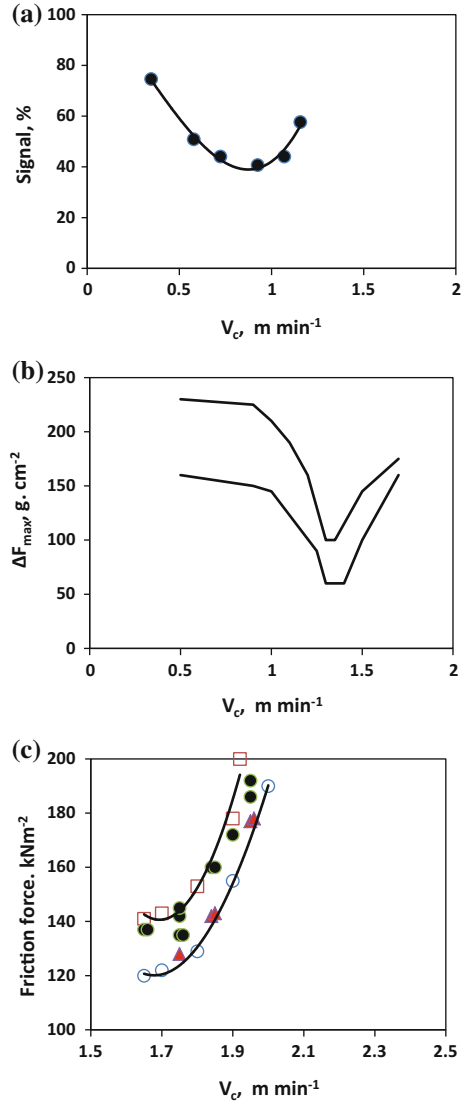
The powder consumption, Q_s , is dependent upon $(V_c)^{-1}$ (Eqs. 2.12–2.14). Using the modified Wolf relation ($Q_s = 0.55/\eta^{0.5} V_c$) to demonstrate the effect of casting speed, it can be seen that Eq. 2.18 can be re-written as

$$F_l = A\eta(V_m - V_c)\rho_l\eta^{0.5}V_c/0.55 \quad (2.20)$$

Similar relations could be derived with other relationships for Q_s . It can be seen from Eq. 2.20 that an increase in casting speed causes a decrease in the $(V_m - V_c)$ term, in addition, to the increase in the V_c term. These conflicting responses to a V_c increase, result in a minimum (V_c^{\min}) in the F_l – V_c plot shown in Fig. 2.21 reported by D’Haeyer [99]. It can be seen that the $(V_m - V_c)$ is dominant at low speeds and the V_c term tends to dominate at higher casting speeds.

Fig. 2.21 Frictional force as a function of casting speed

a friction signal from ML Tektor, **b** ΔF_{\max} and **c** frictional force using two mould powders, Q ($\eta_{1300} = 0.9$ dPas) = \bullet ; R ($\eta_{1300} = 0.8$ dPas) = \blacktriangle [99]; (permission granted, Europ. Comm. Sci. and Tech. Publ., [99])



Tsutsumi et al. [91] carried out simulation experiments and reported that F_1 decreased:

- As casting speed increased ($F_1 \downarrow$ as $V_c \uparrow$) indicating, $V_c < V_c^{\min}$ in their experiments.
- As the liquid slag film thickness (d_l) increased ($F_1 \downarrow$ as $d_l \uparrow$).
- As the velocity gradient ($(V_m - V_c)/d_l$) decreases.
- With the introduction of non-sinusoidal oscillation.

2.4.2.2 Viscosity (η)

According to Eq. 2.20 the liquid frictional force is a function of $(\eta^{1.5})$ and the Ogibayashi [42, 43] relation (Eq. 2.13) leads to F_l exhibiting a dependence on (η^2) . Thus the frictional forces increase with increasing viscosity. Wolf [42] reported a minimum in the $F_l - (\eta^{0.5} V_c)$ plot (Fig. 2.6) at $5 \pm 2 \text{ (dPas)}^{0.5} \cdot \text{m min}^{-1}$; the equivalent plot for the Ogibayashi relation for Q_s leads to a minimum at $2 \pm 1 \text{ dPas} \cdot \text{m min}^{-1}$ as shown in Fig. 2.7c [44].

Hering et al. [104] reported that the liquid frictional force increased with increasing Al_2O_3 content in the casting slag (Fig. 2.22a). This is presumably due to the increase in viscosity with increasing Al_2O_3 content. However, Hering et al. [104] found that this was not always the case, (as can be seen from Fig. 2.22a) and proposed that the friction was affected the nature of the mineralogical phase formed. It is possible that with the *wollastonite/gehlenite* curve in Fig. 2.22b could be explained by a lowering of T_{br} with increasing Al_2O_3 which offsets the effect of increasing viscosity.

Fig. 2.22 Frictional force as function of **a** Al_2O_3 content and **b** viscosity (cited in Pas, thus multiply by 10 for dPas [104]); (permission granted, Stahl Eisen, [104], re-drawn)

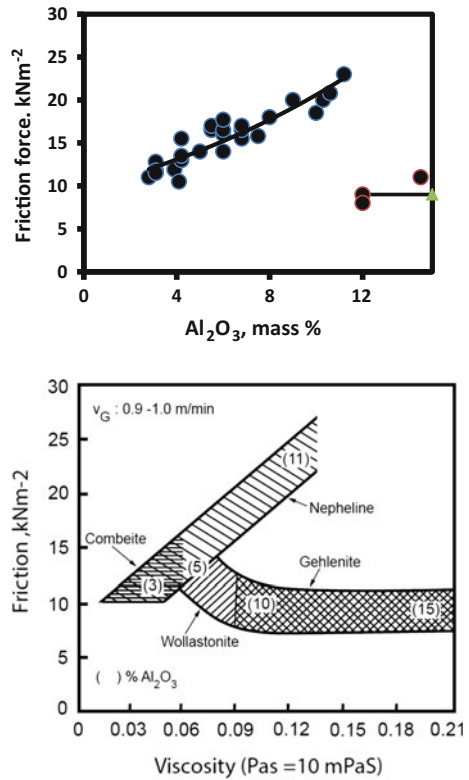
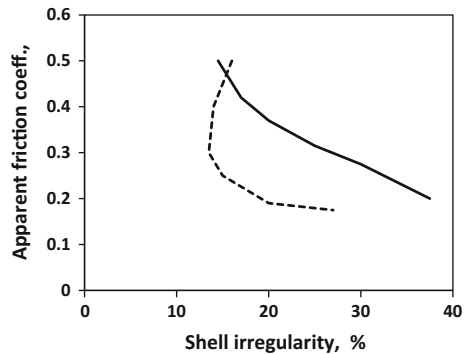


Fig. 2.23 The apparent frictional coefficient as a function of the unevenness (or irregularity) of the shell [105] for $V_c = 2.0$ (—) and 4.0 m min^{-1} (- - -) (permission granted, ISS/AIST, [105])



2.4.2.3 Mould Dimensions and Surface Area (A)

It can be seen from Eq. 2.1 and Fig. 2.20 that the liquid frictional force (F_l) increases as the surface area of the mould (or shell) increases. Ogibayashi et al. [105] pointed out that the shrinkage of the steel will be greatest at the centreline, the point where the shell is at its thinnest. Ogibayashi et al. [105] also pointed out that in *peritectic*, MC steels the shell (in the meniscus region) tends to become uneven or corrugated; this unevenness increases the surface area of the shell. Consequently, the friction coefficient tends to increase as the unevenness of the shell increases (Fig. 2.23).

2.4.2.4 Break (or Solidification) Temperature (T_{br})

Increases in break temperature would be expected to reduce the thickness of the liquid slag film (d_l), as shown in Fig. 2.14; this would result in higher frictional forces ($F_l \uparrow$ as $T_{br} \uparrow$). Furthermore, increasing T_{br} will also enhance the amount of solid friction. Thus on both counts the friction will tend to increase as T_{br} increases.

Measurements of friction and friction coefficient are shown in Fig. 2.24a, b, respectively. These figures show that there is a sharp increase in friction at a temperature slightly below the break temperature, T_{br} ; this may imply that the cooling rates in the friction experiments were slightly higher than those used in the viscosity experiments, since T_{br} decreases with increasing cooling rate. These figures show that relatively small amounts of solid friction can have a significant effect on the total friction. The rate of friction rise was much greater in some cases, denoted. Type A, e.g. Powder J with sharp T_{br} temperatures) than in others (Type B i.e. more “glassy” slags, e.g. Powder A).

2.4.2.5 Frequency (f)

Since most plant observations indicate that powder consumption Q_s decreases as f increases, it is expected that an increase in frequency would increase the liquid

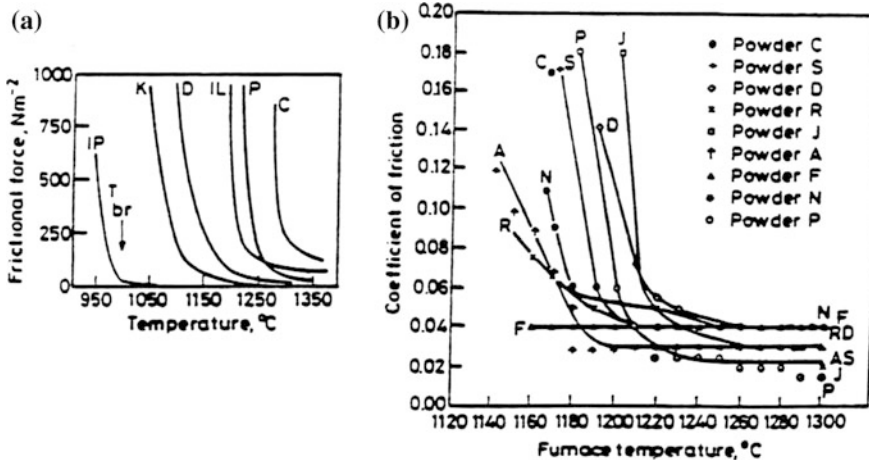


Fig. 2.24 a Frictional force [98] and b Coefficient of friction [27, 103] as functions of temperature derived in rotating cold finger and oscillating pad tests, respectively (permission granted, Europ. Comm. Sci. and Tech. Publ. [27, 98])

friction ($F_1 \uparrow$ as $f \uparrow$). This relationship ($F_1 \uparrow$ as $f \uparrow$) has been confirmed by several investigators [53, 64, 106]. It should be noted that an increase in frequency also increases the velocity of the mould (V_m) and it can be seen from Eq. 2.18 that an increase in V_m will result in an increase in friction.

2.4.2.6 Stroke Length (S)

It can be seen from Table 2.3 that there is no consensus on the effect of the stroke length (s) on the powder consumption, Q_s . The statistical analysis of plant data due to Saraswat et al. [4] indicates that Q_s decreases as the stroke increases ($Q_s \downarrow$ as $s \uparrow$); on this basis, F_1 would be expected to increase (i.e. $F_1 \uparrow$ as $s \uparrow$). Other workers have reported that Q_s increases with increasing stroke ($Q_s \uparrow$ as $s \uparrow$) [53, 64] which would result in ($F_1 \uparrow$ as $s \downarrow$). However, Q_s (or d_1) is not the only factor affecting friction forces and an increased stroke would lead to increased values for V_m and ($V_m - V_c$) and F_1 . Thus no relation between F_1 and s can be recommended at this stage.

2.4.2.7 Negative and Positive Strip Time (T_n and T_p)

As mentioned above, there has been considerable debate as to whether powder consumption occurs in negative strip time or positive strip time. Mathematical models [1, 21, 22] indicate that slag infiltration occurs predominantly in the period when the mould (plus rim) are descending, with the infiltration rate being at its highest in late t_n and early t_p . Thus it may be concluded that increased negative strip would increase Q_s and hence decrease F_1 .

However, Tsutsumi et al. [53, 64] reported that in their simulation experiments that increased positive strip resulted in a decrease in F_l . It has also been reported that the correlation of powder consumption with t_p is stronger than that with t_n [25].

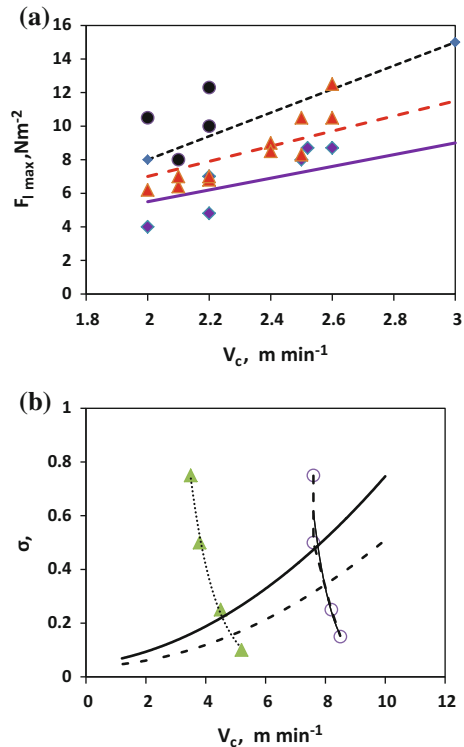
2.4.2.8 Steel Temperature

It has been reported that a decrease in steel temperature results in increased friction measurements, presumably due to the effect of the slag viscosities (which increase at lower temperatures) on the friction.

2.4.2.9 Non-sinusoidal Oscillation

Non-sinusoidal oscillation has been reported to reduce liquid friction [60, 71, 99, 106–108], however, the reverse relation ($F_l \uparrow$ as NSO \uparrow) has been found in trials in Sweden [109]. Mizukami et al. [60] reported that non- sinusoidal oscillation can result in a 40% decrease in liquid friction compared with conventional, sinusoidal oscillation (Fig. 2.25a) but only resulted in a 5% decrease in solid friction (F_s).

Fig. 2.25 Frictional force, F_l , as a function of casting speed **a** showing differences between sinusoidal (---●---) and two modes of non-sinusoidal oscillation (---▲--- and ---◆---) and **b** F_l in relation to tensile strength (σ_B , σ_{suff} , in $N\ mm^{-2}$) denoted in curves, for both the average shell temperature (\blacktriangle) and the surface temperature (o) [60] (permission granted, ISIJ, [60] re-drawn)



Non-sinusoidal oscillation results in a decrease in $(V_m - V_c)$ which leads to a concomitant decrease in the liquid friction (F_l) as shown in Eqs. 2.18 and 2.20. The frictional forces were compared with the tensile strength of the steel (Fig. 2.25a) from which it was concluded that the upper limit for the casting speed when casting with an oscillating mould, lay between 5 and 8 m min⁻¹ [60].

2.5 Summary

The following observations were made concerning the lubrication of the shell and the frictional forces acting on it:

- (i) Inadequate lubrication of the shell leads to various defects in the steel product, such as, longitudinal cracks, sticker breakouts and star cracks.
- (ii) The lubrication is supplied by the liquid slag infiltrating into the channel between mould and shell; this occurs principally in the period where the mould (and slag rim) are descending and Q_s increases gradually through this period with maximum infiltration corresponding with the lowest position of the mould.
- (iii) Changes in mould direction are accompanied by periods of *confused flow* where little slag infiltration occurs.
- (iv) The powder consumption, Q_s (in kg m⁻²) provides a good measure of the lubrication supplied and is related to the thickness of the liquid slag layer in the slag film ($Q_s^{\text{req}} = \rho \cdot d_l$) where ρ is the density of the liquid slag.
- (v) Several powder consumption terms are used and these terms are interrelated; the melting (Q_{MR}) rate must match the required powder consumption.
- (vi) Since mould powders contain carbon and volatile materials it is necessary to distinguish between *powder* and *slag* ($Q_s^{\text{slag}} = f^* Q_s^{\text{powd}}$) where f^* is the mass fraction of the powder forming slag
- (vii) Analyses of plant data for powder consumption revealed that Q_s^{req} increases:
 - with increasing mould surface area, ($Q_s^{\text{req}} = 2/ (R^* - 5)$)
 - with decreasing casting speed and slag viscosity
 - with decreasing oscillation frequency and stroke (although these relations are disputed by some workers); these effects are smaller than those above.
 - with increasing Argon flow rate.
- (viii) The required values of viscosity, break temperature and Q_s^{req} can be calculated for the given casting conditions using empirical rules
- (ix) High frictional forces in the mould arise from (i) fracture of slag films at low casting speeds and (ii) excessive taper and mould misalignment at higher casting speeds
- (x) Liquid friction increases with the:

- Increasing surface area of the shell (including any shell corrugations)
- Increasing viscosity, casting speed and $(V_m - V_c)$; the plot of F_1 versus V_c exhibits a minimum due to the conflicting responses to increasing V_c on $(V_m - V_c)$ and F_1 with $(V_m - V_c)$ dominant at low casting speeds and the V_c effect being dominant at high speeds.
- Increasing oscillation frequency but there is no consensus regarding the effect of stroke length.
- With decreasing non-sinusoidal oscillation.

References

1. P.E. Ramirez-Lopez, K.C. Mills, P.D. Lee, B. Santilanna, *Met. Mater. Trans.* **43**, 109, (2011).
2. A.B. Fox, PhD Thesis, *Mould fluxes their properties and performance*. Dept. of Materials, Imperial College, London, (2003).
3. Y Nuri, T Ohashi, N Miyasaka, K Shima, Y Uchida, *Trans. ISIJ*, **20**, B170, (1980).
4. R. Saraswat, A.B. Fox, K.C. Mills, P.D. Lee, B. Deo, *Scand. J. Met.*, **33**, 85, (2004).
5. T. Kajitani, K. Okazawa, W. Yamada, H. Nakamura, *ISIJ Intl.* **46**, 250, (2006).
6. M.S. Jenkins, PhD Thesis "*Heat transfer in the continuous casting mould*", Monash Univ., Clayton, Vic., Australia, (1999).
7. Y. Itoh, S. Nebeshima, K. Sorimachi, *Proc. 6th Intl. Conf. Molten slags, fluxes and salts*, Stockholm, Paper 152 (2000) see also S. Nebeshima, Y. Itoh, H. Tozawa, H. Nakato, K. Sorimachi, *Proc. 4th Intl. Conf. Solidification Processing*, Sheffield, 1997 (Sheffield Univ., 1997) p 10.
8. K. Tsutsumi, *Tetsu- to Hagane*, **84**, 617, (1998).
9. A. Badri, B.T. Natarajan, C.C. Snyder, K.D. Powers, F.J. Byrne, M. Byrne, A.W. Cramb, *Met. Mater. Trans. B*, **36B**, 355, (2005).
10. A. Badri, B.T. Natarajan, C.C. Snyder, K.D. Powers, F.J. Byrne, M. Byrne, A.W. Cramb, *Met. Mater. Trans B*, **36B**, 373, (2005).
11. EY Ko, J Choi, JY Park, I Sohn, *Met. Mater. Intl.* **20**, 141 and 1103 (2014).
12. E Anzai, T Shigezumi, T Nakano, T Ando, M Ikeda, *Nippon Steel Technical Report*, **34**, 35, (1987).
13. C. Niggel, F. Felder. *Lubrication by slag of continuous casting of steel*. Report 9339, ECSC, (Europ. Comm. Sci and Tech. Publ., Luxembourg, 1985).
14. J. Kor, "An analysis of the fluid flow of liquid mould flux into space between continuous casting mold and steel shell" US Steel Report.
15. Y. Nuri, T. Ohashi, *Trans. ISIJ*, **20**, B172, (1980).
16. S. Ogibayashi, *Proc. 85th Steelmaking Conf.* (2002) (ISS/AIME, Warrendale PA.) p. 175.
17. K. Okazawa, T. Kajitani, W. Yamada, H. Nakamura, *ISIJ Intl.*, **46**, 226 and 234 (2006).
18. K. Schwerdtfeger, K.H. Tacke, *Fundamental study of behaviour of casting powders*; Report EUR 9560, (Europ. Comm.Sci. and Tech Publ., Luxembourg, 1985).
19. YA Meng, BG Thomas, *Met. Mater. Trans. B*, **34B**, 707, (2003).
20. S. Itoyama, *CAMP- ISIJ*, **14**, 893, (2001).
21. P.E. Ramirez-Lopez, K.C. Mills, P.D. Lee, B. Santilanna, *ISIJ Intl.*, **30**, 1797, (2010).
22. C. Ojeda, J. Sengupta, B.G. Thomas, J. Barco, J.L. Aruna, *Proc. AIST Tech.*, 2006 vol 1 (ISS, Warrendale, PA) p. 1017.
23. H.J. Shin, S.H. Kim, B.G. Thomas, G.G. Lee, J.M. Park, J. Sengupta, *ISIJ Intl.*, **46**, 1635, (2006).

24. XN Meng, MY Zhu, Can. Metall. Q, **50**, 45, (2011).
25. ASM Jonayat, BG Thomas, Met. Mater. Trans. B, **45B**, 1862, (2014).
26. T.H. Billany, K.C. Mills, *Mould flux performance during continuous casting*. Final Report ECSC Contract 7210 CA 820, 1987, (Europ. Comm. Sci. and Tech. Publ. Luxembourg, 1987).
27. R.J. Gray, *Behaviour of mould fluxes during continuous casting*. Report EUR 9495 EN 1985) (Europ. Comm. Sci. and Tech. Publ., Luxembourg, 1985).
28. T. Okazaki et al., Tetsu-to Hagane, **65** (10), 265, (1985).
29. JM Hill, YH Wu, B Witwatanapataphee, J Eng. Math., **36**, 311, (1999).
30. S Ogibayashi, CAMP- ISIJ, **18**, 126 and 127 (2003).
31. T Emi, H Nakato, K Suzuki, Y Iida, T Ueda, Tetsu- to Hagane, **60** (7), 981, (1974) Henry Brucher Translation HB9357.
32. T Fastner, C Furst, HP Narzt, G Xia, G Zuba, Proc. 3rd Europ. Conf. Continuous Casting Madrid, (UNESID, Madrid, 1998) p. 791.
33. Y Fukuda, H Kawai, M Okimori, M Hojo, S Tanaka, Proc. 5th Intl. Conf. Slags, Fluxes and molten salts, Sydney, 1997, (ISS, Warrendale, PA, 1997) p. 791.
34. S Ogibayashi, T Mizoguchi, T Kajatani, Intl. Workshop on Thermophys. Data for the Development of Mathematical models of solidification, Gifu City, Japan (1995).
35. BG Thomas, A Moitra, R McDavid, Iron and Steelmaker, **23** (4), 51 (1996).
36. Y. Meng, B.G. Thomas, Proc. ISS Tech., Indianapolis, 2003 (ISS, Warrendale, PA, 2003) p. 589.
37. MS Jenkins Proc. 78th Steelmaking Conf., 1995, (ISS, Warrendale, PA, 1995) p. 669.
38. MS Jenkins, BG Thomas, WC Chen, RB Mahapatra, Proc. 77th Steelmaking Conf., 1994, (ISS, Warrendale, PA 1994) p. 337.
39. JW Kim, S. K. Kim, D. S. Kim, Y. D. Lee, J. I. Eum, E. S. Lee., Proc. 78th Steelmaking Conf. 1995, (ISS, Warrendale, PA, 1994) p. 333.
40. K Suzuki, C Matsumura, H Yamamoto, Y Kanrda, Proc. 73rd Steelmaking Conf., 1990, (ISS, Warrendale, PA, 1990) p 197.
41. M. Wolf, AIME Elect. Furn. Proc., **40**, 335, (1982).
42. M. Wolf, Proc. 2nd Europ. Conf. Continuous Casting, Dusseldorf, 1994 (VDEh, Dusseldorf, 1994) vol 1, p 78.
43. S. Ogibayashi, K Yamaguchi, T Mukat, T Takahashi, Y Mimura, K Koyama. Y Nagano, T Nagano. Nippon Steel Technical Report, **34**, 1, (1987).
44. Y. Nakamori, Y Fujikake, K Tokiwa, T Kataoka, S Tsuneoka, H Misumi, Proc. 10th Conf. IMEKO TC3 on Measurement and Mass held Kobe, Japan Sept. (1984) and Tetsu-to Hagane, **70**(8), 1282, (1984).
45. S. Sridhar, K.C. Mills, V. Ludlow, S.T. Mallaband, Proc. 3rd Europ. Conf. Continuous Casting, Madrid, 1998, (UNESID, Madrid, 1998) p. 807.
46. F Neumann, J Neal, MA Pedroza, AH Castillejos, FA Acosta, Proc. 79th Steelmaking Conf. 1996. (ISS, Warrendale, PA, 1996) p. 249.
47. K.C. Mills, S. Sridhar, A.S. Normanton, S.T. Mallaband, Proc. Brimacombe Conf., Vancouver, BC, 2000, p 781.
48. K.C. Mills, A.B. Fox, ISIJ Intl., **43**, 1479, (2003).
49. H. Maeda, T. Hirose, CAMP-ISIJ, **6**, 280, (1993).
50. K Koyama, K Nagano, Y Nagano, T Nakano, Nippon Steel Technical. Report, **34**, 41, (1987).
51. OD Kwon, J Choi, IR Lee, JW Kim, KH Moon, YK Shin, Proc. 74th Steelmaking Conf., 1991, (ISS, Warrendale, PA, 1991) p. 561.
52. K. Nakajima, S Hiraki, T Kanazawa, T Murakami, CAMP-ISIJ, **5**, 1221, (1992).
53. K. Tsutsumi, H Murakami, S Nishioka, M Tada, M Nakada, M Komatsu, Tetsu- to- Hagane, **84**, 617, (1998).
54. P E Ramirez-Lopez, P.D. Lee, K.C. Mills, ISIJ Intl., **50** (3), 425, (2010).
55. M Kawamoto, T Mizukami, M Hanao, H Kikikuchi, T Watanabe, Ironmaking and Steelmaking, **29**, 199, (2002).

56. K Watanabe, K Tsutsumi, M Suzuki, H Fujita, S Hatori, T Omoto, ISIJ Intl., **54**, 865, (2014).
57. T. Kitagawa, M. Ishiguro, Proc. 4th Japan-Germany Seminar, (ISIJ, Tokyo, 1980) p. 249.
58. T. Kajitani, K. Okazawa W. Yamada, H. Yamamura, ISIJ Intl., **46**, 250 and 1432 (2006).
59. IR Lee, JW Kim, J Choi, D Kwon, YK Shin, Proc. Conf. on Continuous casting in developing countries, Beijing, 1993, (SEAISI, Singapore, 1993) p. 814.
60. T. Mizukami, K Kawakami, T Kitagawa, M Suzuki, S Uchida, Y Komatsu, Trans. ISIJ, **26**, B164, (1986).
61. M Suzuki, H Mizukami, T Kitagawa, K Kawakami, S Uchida, Y Komatsu, ISIJ Intl., **31**, 254, (1991).
62. M. Wolf, “*Effects of mould oscillation*” presented Discussion Group on Continuous casting of mould fluxes, Inst. of Metals, London (1984).
63. M. Wolf, Proc. Conf. Continuous casting of steel in developing countries, Beijing, China (1994) p. 69.
64. K. Tsutsumi, T. Nagasaka, M. Hino, ISIJ Intl., **39**, 1150, (1999).
65. T. Emi, H Nakato, K Suzuki, Y Iida, Proc. NOH- BOS Conf. (1978) p. 350.
66. H. Nakato, I. Muchi, Tetsu-to- Hagane, **66**, 33, (1980).
67. H. Nakato T Sakuraya, T Nozaki, T Emi, H Nikoshawa, *Mould fluxes for continuous casting and bottom pour teeming* (ISS, Warrendale, PA, 1987) p. 23.
68. K. Noguchi, K. Sawamura, Proc. 4th Intl. Conf. Cont. Casting, Brussels (1988) (CRM/VDEh) p. 65.
69. Y. Kobayashi, S. Maruhashi, “Effects of operational on oscillation mark of continuously cast, stainless steel slabs” Proc. 4th Japan-CSSR Seminar, Ostrava. (1983) p. 249.
70. S. Shimizu, Y. Imada et al., Proc. 6th Intl. Iron and Steel Congress (1990) p. 487.
71. M. Suzuki, S Miyahara, T Kitagawa, S Uchida, K Okimoto, Tetsu-to Hagane, **78**, 113, (1992).
72. M Ikeda, K Asano, T Nakano, M Fuji, S Mizoguchi, H Mizumi, Trans. ISIJ, **21**, B 511, (1981).
73. T. Mallaband, Metallurgia. UK, private communication cited in AB Fox thesis [1].
74. T. Mukongo, C Pistorius, A Garbers-Craig, Ironmaking Steelmaking, **31**,135, (2004).
75. Q. Wang, Y. Lu, S. He, K.C. Mills, Z.S. Li, Ironmaking and Steelmaking, **38**, 297, (2011).
76. H Lei, Y Zhao, DQ Geng, ISIJ Intl., **54**, 1629, (2014).
77. T Kishi, H Takeuchi, M Yamamiya, H Tsuboi, T Nakano, T Ando, Nippon Steel Tech. Report, **34**, 11, (1987).
78. M Hanao, Y Tsukaguchi, M Kawamoto, Proc. 4th Intl. Congress Science and Technol., 2008, Gifu, Japan (ISI J, Tokyo, 2008), p. 694.
79. R. Koldwein, Unpublished Corus Internal Rept (2007) cited in KC Mills, J Kromhout, A Hamoen, R Boom: Proc. Admet Conf, Dnipropetrovsk, 2007(Natl. Metall. Acad. Ukr., Dnipropetrovsk, 2007) vol 2 p 174.
80. M Washio, M Sugizawa, S Moriwaki, K Kariyaa, S Idogawa, S Takeuchi, Revue de Metallurgie, CIT, **90** (April), 507, (1993).
81. D W van der Plas, C Platvoet, B Dienesme, JP Radot, JM Galpin, Proc. 2nd Europ. Conf. Continuous casting, Dusseldorf, 1994, Metec Congress’94 (VDEh, Dusseldorf, 1994) p. 109.
82. MY Ha, SG Lee, SH Seong, J. Mater. Processing Technol. **133**, 322, (2003).
83. G Bocher, U Hoffman, P Muller, Proc. 2nd Europ. Conf. Continuous casting, Dusseldorf, 1994, Metec Congress’94 (VDEh, Dusseldorf, 1994)p. 102.
84. J Kromhout, RS Schimmel, Proc. 8th Europ. Conf. Continuous casting, Graz, Austria, 2014 (Austrian Met Mater. Soc., Vienna, 2014).
85. M Tani, T Toh, K Umetsu, K Tanaka, M Zeze, K Tsunenari, K Hayashi, S Fukunaga, Nippon Steel Technical Report, **104**, 62, (2013).
86. JK Park, JW Cho, KH Moon, SH Lee, KH Kim, HS Jeong, Proc. 7th Intl. Conf. Clean Steel, Balatonfured, Hungary, 2007, (Hung. Min. Metall. Soc, Budapest, 2007) p. 264.
87. M. Wolf, Proc. 2nd Europ. Conf. Continuous Casting, METEC Congress’94 held Dusseldorf, 1994 VDEh, Dusseldorf, 1994), vol 1, p 78.

88. H Uchiyama, Proc. AISI Technical Committee on Strand casting, 1995 p.
89. J Sardemann, H Screwe, Stahl u Eisen, **111**, (11), 39, (1991).
90. H Yamamura, T Kajitani, J Nakashima, M Yamasaki, S Mineta, Nippon Steel Technical Report, **104**, 54, (2013).
91. K Tsutsumi, J Ohtake, M Hino, ISIJ Intl., **40**, 601, (2000).
92. H Steinruch, C Rudischer, W Schneider, Non-linear Analysis, Theory, Methods and Applications, **30** (8), 4915, (1997) see also BHM 141 (1996)(9) 399.
93. H Steinruch, C Rudischer, W Schneider Proc. Conf. Modelling of Casting Welding and Advanced Solidification processes VIII (MCWASP)(Minerals, Metals and Materials Soc. 1998).
94. PP Sahoo, S Basu, ISIJ Intl., **46**, 219, (2006).
95. M Wolf, Trans ISIJ, **22**, B204, (1982).
96. TJ Billany AS Normanton, KC Mills, P Grieveson, Ironmaking and Steelmaking **18**, 403, (1991).
97. K. Sorimachi, Proc. 5th Intl. Conf. Molten slags, fluxes and salts, Sydney, 1997, (ISS, Warrendale, PA, 1997) p. 781.
98. PV Riboud, Y Roux, *Fundamental study of the behaviour of casting powders*. Report EUR 9560, 1985 (Eur. Comm. Sci and Tech. Publ., Luxembourg, 1985).
99. R.D. Haeyer, *Influence of chemical composition of continuous casting powders* Report EUR 10326 EN (1987) (Eur. Comm. Sci and Tech. Publ., Luxembourg, 1987).
100. Y Nakamori et al, Nippon Steel Tech. Report, **34**, 53, (1987).
101. B Mairy, D Ramelot, M Dutrieux, Proc. Technol. Conf., Measurement and Control Instrumentation in the Iron and steel Industry, Detroit, 1985 (ISS, Warrendale, 1985) p. 101.
102. G. Saucedo et al, Proc. 74th Steelmaking Conf. (1991) (ISS, Warendale, PA, 1991) p 79.
103. D. Bowen: Proc. Seminar on Mould powders for continuous casting, held British Steel Teesside Laboratories, Sept (1989) Paper 8.
104. L. Hering, HP Heller, HW Fenske., Stahl u Eisen, **17**, 61, (1992).
105. S. Ogibayashi et al, Proc. 78th Steelmaking Conf., Nashville, TN, 1995, (ISS, Warrendale, PA, 1995) p. 451.
106. H Mizukami, M Komatsu, T Kitagawa, K Kawakami, Trans ISIJ, **24**, B 181, (1984).
107. H Mizukami, K Kawakami, S Miyahara, M Suzuki, T Kitagawa, O Terada, Trans. ISIJ, **25**, B 300, (1985).
108. H Mizukami, A Ozeki, A Kurabayashi, N Hsebe, S Uchida, T Kitagawa, Trans ISIJ, **25**, B 301, (1985).
109. T Sohlgren, private communication, Sweden, 2015.

<http://www.springer.com/978-3-319-53614-9>

The Casting Powders Book

Mills, K.C.; Däcker, C.-Å.

2017, XIX, 535 p. 322 illus., 151 illus. in color.,

Hardcover

ISBN: 978-3-319-53614-9